AFRL-OSR-VA-TR-2015-0108

CONTROLLED SYNTHESIS AND FUNCTIONALIZATION OF VERTICALLY-ALIGNED CARBON NANOTUBES FOR MULTIFUNCTIONAL APPLICATIONS

LIMING DAI
CASE WESTERN RESERVE UNIV CLEVELAND OH

05/07/2015
Final Report

Air Force Research Laboratory
AF Office Of Scientific Research (AFOSR)/ RTD
Arlington, Virginia 22203
Air Force Materiel Command

REPORT DOCUMENTATION PAGE

Form Approved
OMB No. 0704-0188

1. REPORT DATE *(DD-MM-YYYY)*	2. REPORT TYPE	3. DATES COVERED *(From - To)*
April 28, 2015	Final Report	May, 2012 – April, 2015

4. TITLE AND SUBTITLE

Controlled Synthesis and Functionalization of Vertically-Aligned Carbon Nanotubes for Multifunctional Applications

5a. CONTRACT NUMBER

5b. GRANT NUMBER
FA9550-12-1-0069

5c. PROGRAM ELEMENT NUMBER

6. AUTHOR(S)

Liming Dai

5d. PROJECT NUMBER

5e. TASK NUMBER

5f. WORK UNIT NUMBER

7. PERFORMING ORGANIZATION NAME(S) AND ADDRESS(ES)

Liming Dai
Case Western Reserve University
10900 Euclid Avenue
Cleveland, Ohio 44106

8. PERFORMING ORGANIZATION REPORT NUMBER

CON119472

9. SPONSORING / MONITORING AGENCY NAME(S) AND ADDRESS(ES)

Dr. Charles Lee
AFOSR/NA
875 North Randolph, Street
Suite 325, Room 3112
Alexandria, VA 22203

10. SPONSOR/MONITOR'S ACRONYM(S)
AFOSR

11. SPONSOR/MONITOR'S REPORT NUMBER(S)

12. DISTRIBUTION / AVAILABILITY STATEMENT

(see next page)
DISTRIBUTION STATEMENT A

13. SUPPLEMENTARY NOTES

NIL

14. ABSTRACT

As we proposed originally, the objective of the project is to synthesize and functionalize vertically-aligned carbon nanotubes (VA-CNTs) for multifunctional applications. Along with the development of advanced CVD and solutions method for controlled synthesis of VA-CNTs, we have also develop leading-edge functionalization strategies to prepare VA-CNT with various tailor-made architectures/structures for a large variety of applications, including energy- (*e.g.*, supercapacitors, batteries, solar cells, fuel cells) and bio-related devices (*e.g.*, biosensors, biomimetic dry adhesives)**.** This project has led to more than 40 journal publications, including *Nature Nanotechnology* (2), *Angew. Chem. Int. Ed.* (2), *Advanced Materials* (5), *Energy Environ. Sci.* (2), *ACS Nano* (3), *Nano Lett.* (1), *Acc. Chem. Res.* (1), and *Chem. Rev.* (1), 3 book chapters, and received numerous commentaries appeared in scientific, business, and popular press (please see: "Events & News" at http://case.edu/cse/eche/daigroup/news.html and many others on internet).

15. SUBJECT TERMS

16. SECURITY CLASSIFICATION OF:			17. LIMITATION OF ABSTRACT	18. NUMBER OF PAGES	19a. NAME OF RESPONSIBLE PERSON
a. REPORT	b. ABSTRACT	c. THIS PAGE		31	19b. TELEPHONE NUMBER *(include area code)*

Standard Form 298 (Rev. 8-98)
Prescribed by ANSI Std. Z39.18

Final Performance Report

Project Title: Controlled Synthesis and Functionalization of Vertically-Aligned Carbon Nanotubes for Multifunctional Applications

Contract Number: AFOSR (FA9550-12-1-0069)

Report Title: Final Performance Report

Report Period: May 1, 2012 – April 30, 2015

Funding Organization: AFOSR

Prepared by: Dr. Liming Dai
Principal Investigator
Case Western Reserve University
10900 Euclid Avenue
Cleveland, Ohio 44106
Tel: (216) 368 4151
Liming.dai@case.edu

Prepared for: Dr. Charles Lee
Program Manager
AFOSR/NA
875 North Randolph Street
Suite 325, Room 3112
Alexandria, VA 22203
(703) 696-7779
charles.lee@afosr.af.mil

ABSTRACT

As we proposed originally, the objective of the project is to synthesize and functionalize vertically-aligned carbon nanotubes (VA-CNTs) for multifunctional applications. Along with the development of advanced CVD and solutions method for controlled synthesis of VA-CNTs, we have also develop leading-edge functionalization strategies to prepare VA-CNT with various tailor-made architectures/structures for a large variety of applications, including energy- (*e.g.*, supercapacitors, batteries, solar cells, fuel cells) and bio-related devices (*e.g.*, biosensors, biomimetic dry adhesives)**.** This project has led to more than 38 journal publications, including *Nature Nanotechnology* (2), *Angew. Chem. Int. Ed.* (2), *Advanced Materials* (3), *Energy Environ. Sci.* (1), *ACS Nano* (3), *Nano Lett.* (1), *Acc. Chem. Res.* (1), and *Chem. Rev.* (1), 3 book chapters, and received numerous commentaries appeared in scientific, business, and popular press (please see: "Events & News" at http://case.edu/cse/eche/daigroup/news.html and many others on internet).

TABLE OF CONTENTS

I. ACCOMPLISHMENTS AND NEW FINDINGS

1. SUMMARY OF ACCOMPLISHMENTS ON CONTROLLED SYNTHESIS AND FUNCTIONALIZATION OF VERTICALLY-ALIGNED CARBON NANOTUBES FOR ENERGY APPLICATIONS

1.1 Vertically Aligned BCN Nanotubes with High Capacitance (*ACS Nano* **2012**, *6*, 5259.)

Using a chemical vapor deposition (CVD) method, we have synthesized vertically-aligned BCN nanotubes (VA-BCNs) on Ni-Fe coated SiO_2/Si substrate from melamine diborate precursor. The effects of pyrolysis conditions on the morphology and thermal property of grown nanotubes, as well as the nanostructure and composition of an individual BCN nanotube were systematically studied. It was found that nitrogen atoms are bonded to carbons in both graphitic and pyridinic forms, and that the resultant VA-BCNs grown at 1000°C shows the highest specific capacitance (321.0 F/g) with an excellent rate capability and high durability in respect to non-aligned BCN (167.3 F/g) and un-doped multiwalled carbon nanotubes (117.3 F/g) due to synergetic effects arising from the combined co-doping of B and N in CNTs and well-aligned nanotube structure.

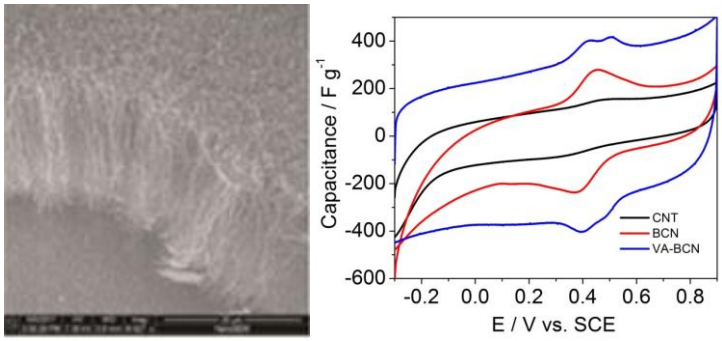

Figure 1. (a) SEM image of VA-BCN nanotubes (scale bar 20 μm). (b) CV curves of CNT (black), BCN (red), and VA-BCN (blue) samples in 1 M H_2SO_4 solution at a scan rate of 5 mV/s with a wide potential window. (adapted from *ACS Nano* **2012**, *6*, 5259).

1.2 Carbon Nanomaterials for High-Performance Supercapacitors (*Materials Today* **2013**, *16*, 272.)

Having a high surface area and relatively low cost, activated carbons have been widely used as electrode materials in commercial supercapacitors. However, currently available activated carbon materials have a low mesoporosity, and hence the limited capacitance due to a low electrolyte accessibility. In order to improve the performance of the state–of–the–art supercapacitors to meet stringent requirements for specific applications (*e.g.*, hybrid electric vehicles; portable, transparent and wearable electronics), new electrode materials having superior properties with respect to the activated carbon electrodes are needed and new device structures are highly desirable. Recently, carbon nanomaterials (especially, carbon nanotubes and graphene) have been widely investigated as effective electrodes in supercapacitors due to their high specific surface area, excellent electrical and mechanical properties. Although supercapacitors based on carbon nanomaterials have achieved higher power densities than those attainable by activated carbon–based commercial capacitors, their energy density still needs to be improved. In conjunction with rational strategies for nanomaterials engineering, the rich chemistries available for controlled functionalization of both carbon nanotubes and graphene have facilitated the development of high-performance supercapacitors based on carbon nanomaterials with unique structures. This invited article summarizes the recent progresses on the development of high–performance supercapacitors based on carbon nanomaterials, including supercapacitors based on our vertically-aligned carbon nanotubes (VA-CNTs) and their derivatives.

1.3 High-Performance Transparent and Stretchable All-Solid Supercapacitors Based on Highly Aligned Carbon Nanotube Sheets (*Sci. Rep.* **2014**, *4*, 3612.)

By using highly aligned carbon nanotube (CNT) sheets of excellent optical transmittance and mechanical stretchability as both the current collector and active electrode, high-performance transparent and stretchable all-solid supercapacitors with a good stability were developed. A transmittance up to 75% at the wavelength of 550 nm was achieved for a supercapacitor made from a cross-over assembly of two single-layer CNT sheets. The transparent supercapacitor has a specific capacitance of 7.3 F g^{-1} and can be biaxially stretched up to 30% strain without any obvious change in electrochemical performance even over hundreds stretching cycles.

Figure 2A(a) schematically shows the procedures for preparing the transparent and stretchable supercapacitors. To start with, we synthesized a vertically-aligned multiwalled carbon nanotube (VA-CNT) forest through chemical vapor deposition of ethylene onto a silicon wafer pre-coaed with Fe (1.2 nm)/Al_2O_3 (3 nm) under a mixture of argon and hydrogen (flow rate of 400 sccm/30 sccm) as the carrier gas at 750 °C. We then continuously drew a transparent CNT sheet out from the CNT forest onto a preformed PDMS substrate (Figure 2A(a)), followed by coating a solution of polyvinyl alcohol (PVA) and H_3PO_4 on the CNT sheet (Figure 1A(a)). Finally, we constructed the supercapacitors by assembling another PDMS-supported CNT electrode on top of the newly-formed PVA-H_3PO_4/CNT/PDMS multilayer film in either a parallel (Figure 2A(b)) or cross (Figure 2A(c)) configuration, leading to highly transparent devices to be seen through even with the naked eye (Figures 2A(b and c)). The resultant supercapacitors are also flexible and stretchable characteristic of the PDMS-supported aligned CNT sheets. The whole device can be bent, folded, and even stretched at least up to 30% strain (Figures 2A(d and e)) without any obvious performance change.

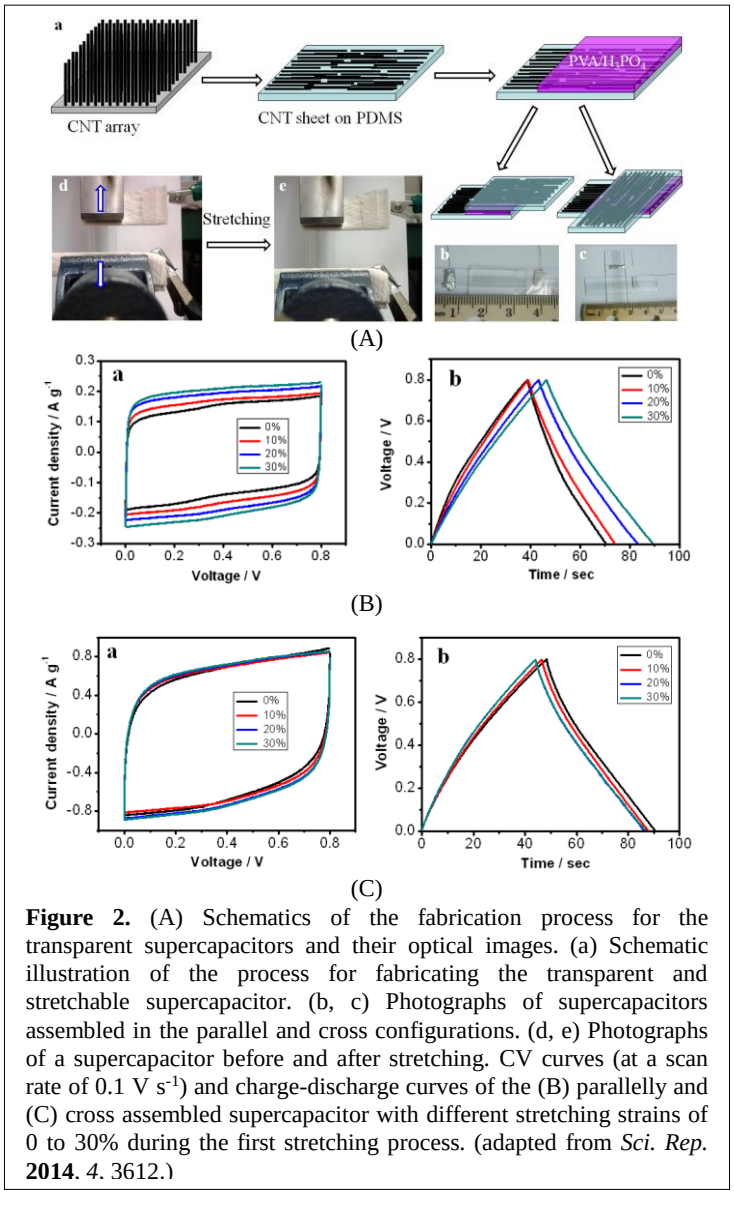

Figure 2. (A) Schematics of the fabrication process for the transparent supercapacitors and their optical images. (a) Schematic illustration of the process for fabricating the transparent and stretchable supercapacitor. (b, c) Photographs of supercapacitors assembled in the parallel and cross configurations. (d, e) Photographs of a supercapacitor before and after stretching. CV curves (at a scan rate of 0.1 V s^{-1}) and charge-discharge curves of the (B) parallelly and (C) cross assembled supercapacitor with different stretching strains of 0 to 30% during the first stretching process. (adapted from *Sci. Rep.* **2014**, *4*, 3612.)

1.4 High-Performance, Extremely Stretchable, Wire-Shaped Supercapacitors (*Angew. Chem. Int. Ed.* **2015**, *54*, 618.)

Using the vertically-aligned carbon nanotube array as the starting materials (Figure 3A(b)), we developed a general approach toward extremely stretchable and highly conductive electrodes by wrapping a continuous carbon nanotube (CNT) thin film around pre-stretched elastic wires, from which high-performance, extremely stretchable wire-shaped supercapacitors were fabricated by twisting two such CNT-wrapped elastic wires pre-coated with poly(vinyl alcohol)/H_3PO_4 hydrogel as the electrolyte and separator. The resultant wire-shaped supercapacitors exhibited an extremely high stretchability up to 350% strain (figure 3B(e)) with a high device capacitance up to 30.7 F g^{-1} - two times that of the state-of-the-art stretchable supercapacitor under only 100% strain. The wire-shaped structure facilitated the integration of multiple supercapacitors into a single wire device to meet specific energy and power needs for various potential applications. These supercapacitors can be repeatedly stretched from 0 to 200% strain for hundred cycles with no change in performance (Figure 3B), outperformed all the reported state-of-the-art stretchable electronics.

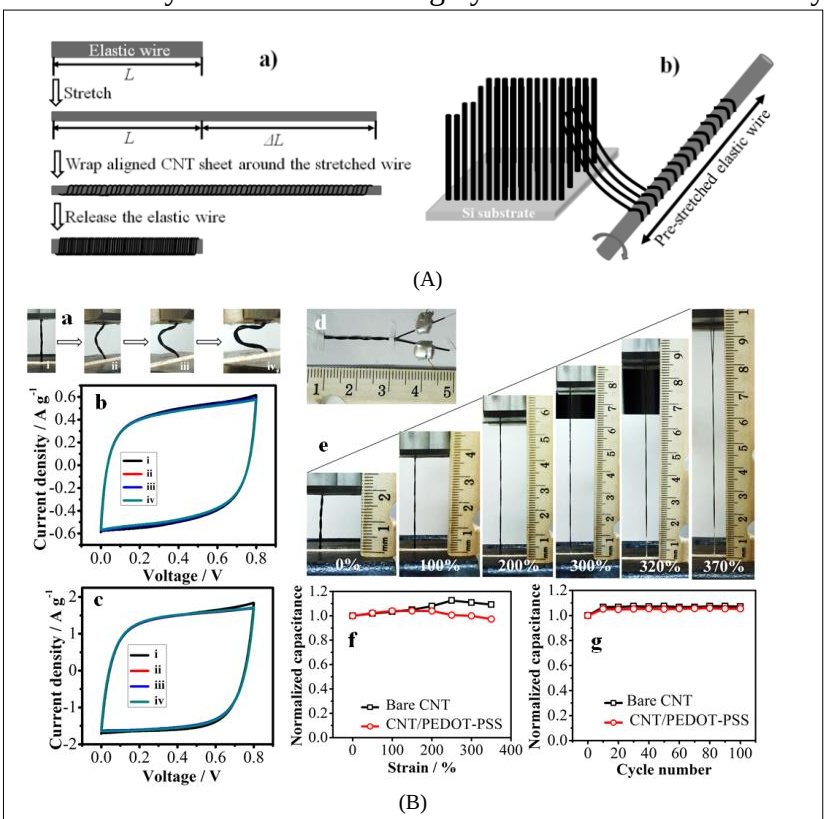

Figure 3. (A) a), b) Schematic illustration of fabricating stretchable conducting wire by wrapping aligned CNT sheet around a pre-stretched elastic wire (64% polyester and 36% polyurenthane). (B) a) The wire-shaped supercapacitors at different bending states. b), c) CV curves of the supercapacitors based on the bare CNT-wrapped (b) and CNT/PEDOT-PSS-wrapped (c) elastic wire electrodes under bending deformations at different bending states shown in (a). A typical wire-shaped supercapacitor with a twisted structure (d) before and e) after being stretched from 0% to 370% strains. Changes in the normalized capacitance f) as a function of the tensile strain and g) as a function of the stretching cycle number; for each of the cycles the supercapacitor was stretched up to 200 % strain and the strain was fully released at the end of each stretching. (adapted from *Angew. Chem. Int. Ed.* **2015, *54*,** 618.)

1.5 Scalable Synthesis of Hierarchically-Structured Carbon Nanotube-Graphene Fibres for Capacitive Energy Storage (*Nat. Nanotechnol.* **2014**, *9*, 555.)

Micro-supercapacitors are promising to complement and even replace batteries for miniaturized portable electronics and microelectromechanical systems. However, they are still suffered from their low energy densities, particularly the volumetric energy density. Using the capillary chromatography column as a one-dimensional hydrothermal micro-reactor, we developed, in collaboration with an international team, a scalable method to continuously produce carbon microfibers with hierarchy structures, in which nitrogen-doped reduced graphene oxide (rGO) and acid-oxidized single-walled carbon nanotubes (SWCNTs) self-assembled into an interconnected SWCNT network with rGO sheets interposed along the microfiber axis to create a mesoporous microstructure of a large specific surface area (396 m^2/g) and a high electrical conductivity (102 S/cm). The resultant carbon hybrid fiber showed ultrahigh specific volumetric capacity of 305 F/cm^3 (at 73.5 mA/cm^3 by three-

electrode cell) in H_2SO_4 or 300 F/cm^3 (at 26.7 mA/cm^3 by two-electrode) in a polymer gel electrolyte (PVA/H_3PO_4). The corresponding fiber-shaped all-solid-state flexible micro-supercapacitors with the PVA/H_3PO_4 electrolyte, but without binder, current collector, or separator, exhibited a long cycle life and an ultrahigh high volumetric energy density of ~6.3 mWh/cm^3. This value of volumetric energy density is well comparable to a 4V/500-μAh thin-film lithium battery, while the power density of our micro-supercapacitors is more than two orders of magnitude higher than the battery. These newly-developed fiber-shaped flexible micro-supercapacitors can be easily integrated into miniaturized power sources for various portable flexible optoelectronics, multifunctional textiles, sensors, and energy devices, as exemplified by powering a TiO_2-based UV photodetector and a commercial light-emitting-diode.

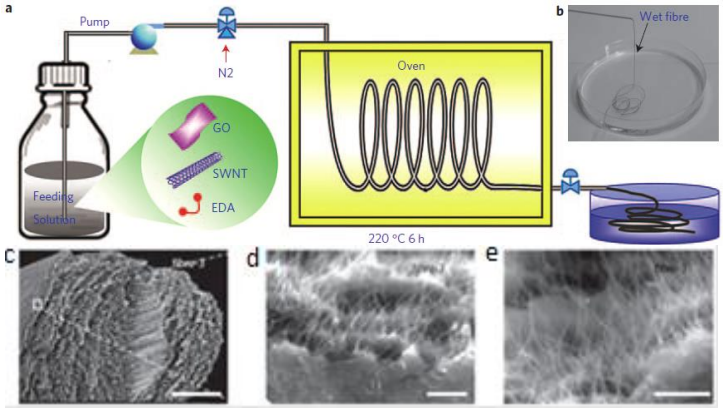

Figure 4. Schematic illustration of the synthesis process for carbon hybrid micro-fibers. (a) The synthesis of fibers using GO, acid-oxidized SWCNT, and EDA as starting materials and flexible fused silica capillary column as hydrothermal reactor. (b) Photo of collecting fibers in water. SEM images of the cross section of the GCF-3 fiber. SEM images of (c) the cross section of the GCF-3 fiber, (d) a square area highlighted in (c), and (e) SWCNT bundles attached to the edges and surfaces of rGO sheets. Scale bars: 15 μm for (c); 0.5 μm for (d); 100 nm for (e). (adapted from *Nat. Nanotechnol.* **2014**, *9*, 555.).

As shown in Figure 4a, the homogeneous solution containing acid-oxidized SWCNT, GO, and EDA was pumped (peristaltic pumper, Shimadzu, LC-20AT) into a flexible fused silica column, which was placed in an oven at 220 °C, for 6 hours before a continuous fiber was pushed into a water reservoir by a pressurized nitrogen flow (Figure 4b). To identify the optimum composition of hybrid fibers for the SC application, several fibers with different SWCNT/GO mass ratios of 0:1, 1:8, 1:4, and 1:1 (denoted as: GF, GCF-1, GCF-2, and GCF-3, respectively) were produced. The fused silica capillary column could be used repeatedly, and the diameter of the continuous hybrid fibers was limited only by the size of the capillary column. The as-prepared dry fibers exhibited a good mechanical strength (84–165 MPa). They are also flexible, and can be bend into different shapes.

A high packing density and large ionic-accessible surface area are two prerequisites for supercapacitor electrodes to achieve high volumetric performances. Thus, it is important to note that both the density and the surface area of the SWCNT/graphene hybrid fibers increased with increasing SWCNT fraction due to the aforementioned unique multi-scale hierarchical structure, as revealed by electron microscopy. Scanning electron microscopy (SEM) images (Figure 4c) show that the GCF-3 fiber has densely-stacked rGO sheets aligning along its main axis. Under higher magnifications, SEM images of the hybrid microfibers further display an interconnected porous structure (Figure 4d, e), which show that SWCNTs perpendicularly aligned between the graphene layers to not only reduce the stacking of the rGO sheets but also provide well-developed porosity in the hybrid microfibers. As a result, the GCF-3 microfiber has a specific surface area of 396 m^2/g, which is much higher than those of other carbon-based micro-fibers reported so far.

Taking the advantages of its good flexibility, high conductivity, and large specific volumetric capacitance, we used the GCF-3 microfiber as both active materials and current collectors to construct flexible supercapacitors. In a typical all-solid-state micro-supercapacitor (Figure 5a), two parallel GCF-3 microfiber electrodes were mounted onto a flexible polyester (PET) substrate using polyvinyl alcohol (PVA)-H_3PO_4 gelled electrolyte without binder, current collector, separator, or any packaging material. Apart from serving as the electrolyte, the polymer gel wrapping the two

fibers also worked as an effective separator to prevent any undesirable short circuit between the two electrodes. The CV curves of the micro-supercapacitor at scanning rates between 5 and 100 mV s^{-1} have an almost rectangular shape in the voltage range of 0–1 V. Its galvanostatic charge-discharge curves (Figure 5b) at the current density of 66.7–133.3 mA/cm^3 have a triangular shape, indicating excellent reversibility and good charge propagation between the two fiber electrodes. Figure 5c illustrates that the volumetric capacitance of the micro-supercapacitor (normalized to the device volume) is ~45.0 F cm^{-3} at ~26.7 mA cm^{-3} and ~25.1 F cm^{-3} at ~800 mA cm^{-3}, corresponding to the area capacitance of ~116.3 mF cm^{-2} and ~64.6 mF cm^{-2}, respectively, outperformed all previously reported carbon-based micro-supercapacitors. The specific volumetric capacitance of single fiber electrode based on the two-electrode cell was calculated to be about 300 F cm^{-3} at ~26.7 mA cm^{-3}. Figure 5d shows that the micro-supercapacitor retained 93 % of its initial capacitance after 10,000 charge-discharge cycles, demonstrating impressive performance stability and fast charging/discharging rates with a long cycle life.

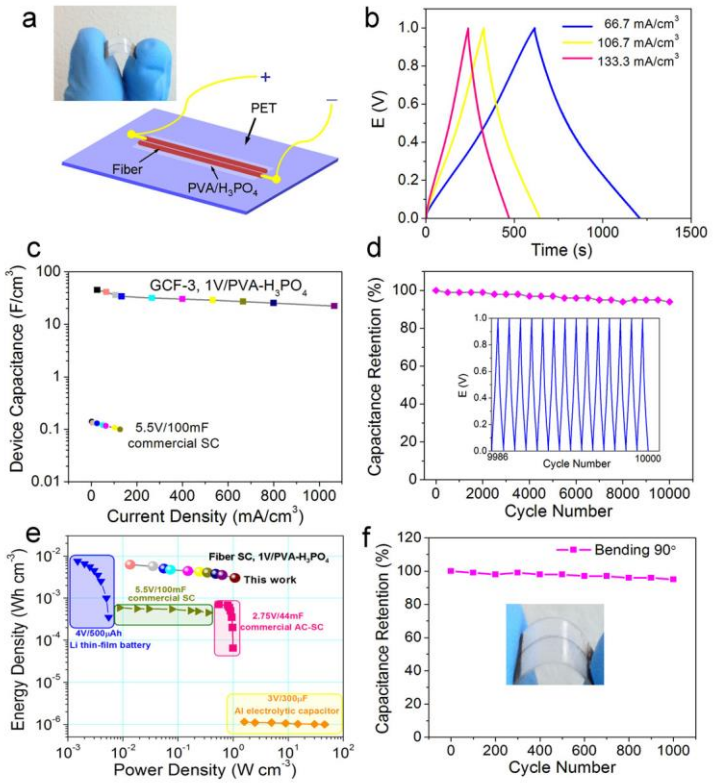

Figure 5. Electrochemical performance of all-solid-state micro-supercapacitors. (a) Schematic illustration and photo of a micro-supercapacitor constructed using two GCF-3 fibers. (b) Galvanostatic charge-discharge curves at various current densities. (c) The volumetric device capacitance at different current densities. Data obtained from a commercial activated carbon supercapacitor are also shown for comparison. (d) Cycle life of the micro-SC and the inset shows the galvanostatic charge-discharge curve after 10,000 cycles between 0–1 V at 250 mA cm^{-3}. (e) Energy and power densities of the miro-SC compared with commercially available state-of-the-art energy-storage systems. Data for the Li battery are from Ref. 1 and data for the 2.75V/44 mV AC-supercapacitor are reproduced from Ref. 6. (f) The capacitance retention after 1,000 cycles up to 90° bending angle. (adapted from *Nat. Nanotechnol.* **2014**, *9*, 555.)

Compared with the gravimetric power/energy density based on active electrode materials, the volumetric power/energy density of the whole supercapacitor is more important for evaluating the energy storage performance of micro-supercapacitors. The Ragone plots (Figure 5e) compare the volumetric performance of our hybrid fiber micro-supercapacitor to that of the commercially available state-of-the-art energy-storage devices. Our micro-supercapaciotr shows the highest volumetric energy density (normalized to the device volume) of ~6.3 mWh/cm^3. The maximum volumetric power density of our micro-supercapacitor is 1085 mW/cm^3, which is comparable to the typical value of commercially available supercapacitors and more than two orders higher than that of lithium thin film batteries. To the best of our knowledge, the volumetric energy density demonstrated in this work is the highest value among all carbon-based solid-state micro-supercapacitors reported to date. However, it should be noted that the PVA-H_3PO_4 electrolyte with a voltage window of 1 V was used in this work. We expect that the use of high-voltage electrolytes, such as ionic liquids, should further increase the energy density. The micro-SC was further subjected to mechanical bending tests to demonstrate the device flexibility for potential applications in flexible electronics. After 1,000 bending cycles at 90°, the device capacitance retention remained above 97%, demonstrating a high flexibility and electrochemical stability (Figure 5f).

1.6 Lithium-Ion Batteries Based on Vertically-Aligned Carbon Nanotube Electrodes and Ionic Liquid Electrolytes (*PhysChemChemPhys* **2012**, *14*, 12099.)

In conjunction with environmentally benign ionic liquid electrolytes, vertically-aligned carbon nanotubes (VA-CNTs) sheathed with and without a coaxial layer of vanadium oxide (V_2O_5) were used as both cathode and anode, respectively, to develop high-performance and high-safety lithium-ion batteries. As schematically shown in Figure 6, we have used VA-CNTs sheathed with and without a coaxial layer of vanadium oxide (V_2O_5) as both cathode and anode, respectively. This is the first time that VA-CNTs were used as both cathode and anode in a Li-ion battery. We found that the VA-CNT anode and the V_2O_5-VA-CNT composite cathode showed a high capacity (600 mAh/g and 368 mAh/g, respectively) with a high rate capability in the ionic liquid electrolyte (*i.e.*, N-Ethyl-N,N-dimethyl-2-methoxyethylammonium bis(trifluormethylsulfonyl)imide, [EDMMEA][TFSI]) used in this study, and that the resultant battery test cells showed a high energy density (297 Wh/kg) and power density (12 kW/kg) (estimated from active-material-based performances), possessing the potential to significantly outperform the current state-of-the-art Li-ion battery technology. Furthermore, the use of ionic liquid electrolytes with superior safety-related properties ensures a high safety and long lifetime for the newly-developed batteries based on the VA-CNT electrodes and ionic liquid electrolytes. To the best of our knowledge, this is the first time that the multiple drawbacks (*e.g.*, the energy storage, power delivery, safety, and lifetime) associated with the current Li-ion batteries are addressed simultaneously in a single battery system, opening up a new approach in developing high-performance Li-ion batteries.

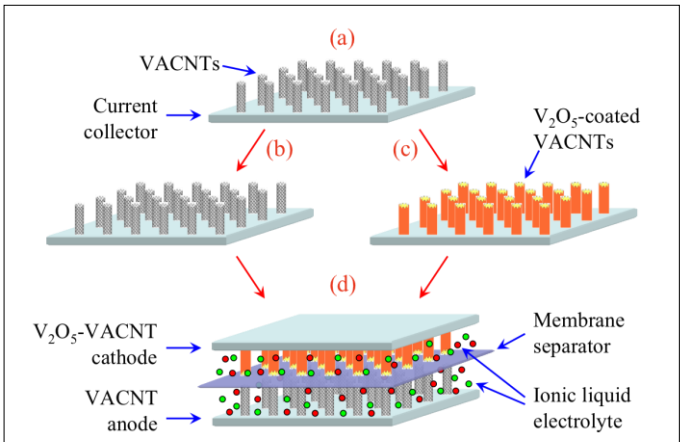

Figure 6. Schematic representation of a Li-ion battery incorporating vertically-aligned carbon nanotube (VA-CNT) electrodes and ionic liquid electrolyte. (a) Growth of VA-CNTs on a conductive substrate (as current collector). (b) Direct use of VA-CNTs as the anode. (c) Deposition of V_2O_5 on VA-CNTs to synthesize V_2O_5-VA-CNT composite cathode. (d) Assembly of the VA-CNT anode, the V_2O_5-VA-CNT cathode, a membrane separator, and an ionic liquid electrolyte to fabricate the battery. High capacity and high rate capability of the VA-CNT anode and the V_2O_5-VA-CNT cathode ensure a high energy density and a high power density, while superior safety-related properties of ionic liquid electrolytes ensure high safety and long lifetime for the battery thus prepared. (adapted from *PhysChemChemPhys* **2012**, *14*, 12099.).

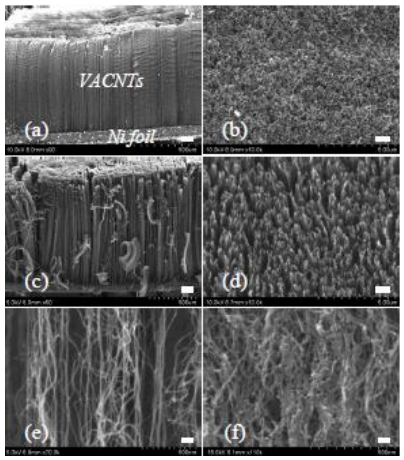

Figure 7. SEM images of a VA-CNT electrode (a, b) before and (c, d) after water plasma etching. (a, c) side view; (b, d) top view, and a plasma-etched VA-CNT electrode before (e) and after (f) deposition of V_2O_5. Scale bar: (a–d) 100 μm, (e-f) 100 nm.. (adapted from *PhysChemChemPhys* **2012**, *14*, 12099.).

To minimize the interfacial electrochemical resistance and enhance the interfacial mechanical strength, we directly grew VA-CNTs onto a Ni foil substrate (as the current collector) that was pre-coated with a thin binary layer of Fe (3 nm)/Al (10 nm) as the catalyst for the nanotube growth. The VA-CNT growth was performed by chemical vapor deposition of a gas mixture of 48% Ar, 28% H_2, 24% C_2H_2 at 750°C for 10-20 minutes. The metal-substrate-supported nanotube growth also ensured the direct use of the resultant VA-CNT/Ni assembly as the electrode, eliminating completely a time-consuming procedure for the electrode preparation with CNTs being transferred from insulting substrates (*e.g.*, SiO_2/Si wafers) typically used for the nanotube growth. Figures 7a&b show the well-aligned VA-CNTs with a thin top layer of randomly oriented nanotube segments grown on the Ni foil substrate. Upon plasma etching, the top nonaligned carbon layer was removed

whilst largely retaining the structural integrity of the vertically-aligned nanotube trunks (Figures 7c, d). On the other hand, the H_2O-plasma etching also led to a more opened morphology for VA-CNTs (compare (d) with (b) of Figure 7), due possibly to the water-plasma-induced segregation of the nanotubes, to facilitate the electrochemical deposition of V_2O_5 and the electrolyte access into the nanotube electrode (Figure 7e, f). The plasma-etched VA-CNT electrode had a tube loading density of ~1.5 mg/cm^2, a tube length of ~ 600 μm, a tube diameter of 10 ~ 15 nm, and a tube spacing of tens to hundreds of nanometers.

In the present work, we used cyclic voltammetry to study the Li^+ intercalation/deintercalation characteristics and reversibility and used galvanostatic charging/discharging tests to study the rate capability of our electrode materials. Figure 8a shows well-defined cyclic voltammograms (CVs) for a plasma-etched VA-CNT electrode (as anode) in 1 M LiTFSI/20% EC/[EDMMEA][TFSI]. During the first cathodic scan, an irreversible reduction peak attributable to the reduction of ethylene carbonate appeared at 1.2 V and then disappeared in the following scans due to the formation of a stable SEI film on the VA-CNT electrode. At the first CV cycle, the columbic efficiency defined by the ratio of oxidation charge to reduction charge of the VA-CNT electrode is low (Figure 8b). This should be due to the SEI formation as typically observed at a conventional graphite anode. The low efficiency observed here is believed to be caused by the high surface area of CNTs. Further cycling led to a stable and reversible Li^+ intercalation (at 0 V)/deintercalation (at 0.35 V), and thus an improved columbic efficiency. After 5 cycles, the columbic efficiency reached 98%, indicating a highly reversible Li^+ intercalation/deintercalation process for the VA-CNT electrode, which can be clearly seen in the inset of Figure 8b. The formation of a stable SEI film and the reversibility of the Li^+ intercalation/deintercalation are essential for a high-performance Li-ion battery anode. Therefore, the plasma-etched VA-CNTs developed on the present study, in conjunction with the ionic liquid electrolyte, are good anode materials for advanced Li-ion batteries. Plasma etching has further removed the top nonaligned carbon layer and led to a more porous morphology for the VA-CNT electrode (Figures 7b&d), which could significantly enhance the Li^+ intercalation/deintercalation process associated with the VA-CNT anode. Indeed, the plasma-etched VA-CNT anode showed much higher and more reversible Li^+ intercalation/deintercalation currents than the pristine VA-CNT anode.

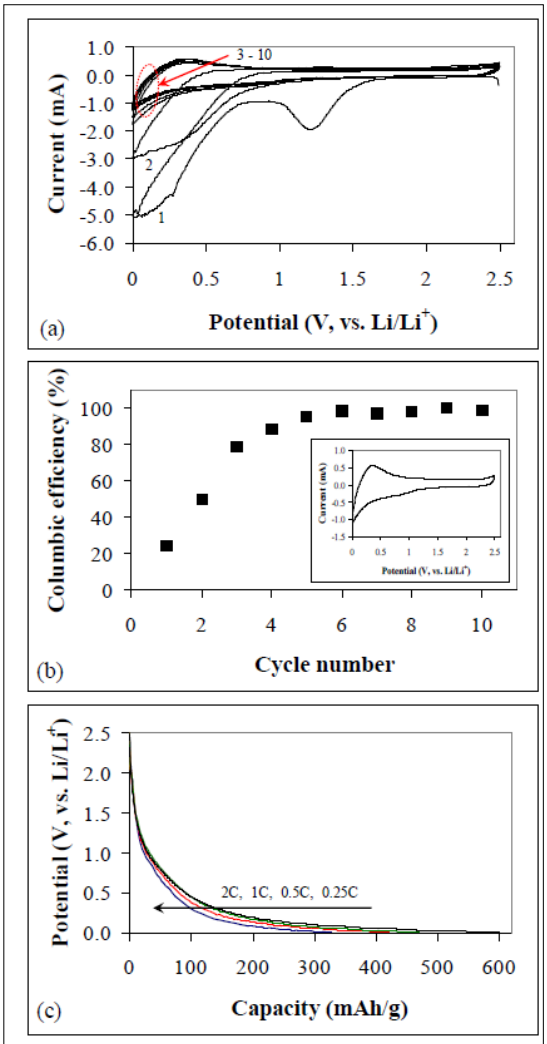

Figure 8. a) Cyclic voltammograms (CVs) and corresponding columbic efficiency: (a) CVs and (b) corresponding columbic efficiency of a plasma-etched VA-CNT electrode recorded in 1 M LiTFSI/20% EC/[EDMMEA][TFSI] electrolyte. Scan rate: 1 mV/s. The number in (a**)** represents the number of cycles. The inset in (b) is the 10th cycle of the CV. (c) Discharge curves of the plasma-etched VA-CNT electrode recorded at the rates increasing from 0.25C to 2C as indicated by the arrow (curves shown were from the third cycle at each rate). Cut-off potential: 0 - 2.5V. Galvanostatic charging/discharging (c) was performed for a same VA-CNT electrode after its CV test (a). (adapted from *PhysChemChemPhys* **2012**, *14*, 12099.).

During the galvanostatic charging/discharging at a relatively low rate of 0.25C, the VA-CNT anode showed a typical Li^+ intercalation plateau at around 0 V, corresponding to a high reversible capacity of 600

mAh/g (Figure 8c). Upon the increase in discharge rate, a gradually decreased capacity was observed as expected (*e.g.*, 0.5 C: 471 mAh/g, 1 C: 422 mAh/g). Nevertheless, at a rate as high as 2C, the VA-CNT anode retained the capacity at 365 mAh/g with a capacity retention up to 61 %, indicating a high rate capability. It should be noted that considerable research has been reported in the literature about the development of high-rate Li^+ intercalation anode (mostly with conventional electrolytes). Taking into account the relatively higher viscosity and lower conductivity of ionic liquids compared to conventional electrolytes, the rate performance of our VA-CNT anode in the present work should be considered to be reasonably high, which should be attributed to the unique porous structures of the VA-CNTs. As illustrated in Figure 6, each of the constituent aligned tubes of a VA-CNT electrode is directly connected onto a common current collector. The vertically-aligned nanotubes with a well-defined large surface area, high mesoporosity, and intimate contact to the current collector should allow for a rapid charge/discharge process collectively through each of the individual nanotubes within the VA-CNT electrode. Therefore, the high-rate capability of the VA-CNTs for Li^+ intercalation/deintercalation could ensure a high power for Li-ion batteries. Furthermore, a separate continuous charging/discharging test (up to 100 cycles) did not show significant capacity degradation for the VA-CNT electrode, indicating its good stability as anode in the ionic liquid electrolyte selected.

Anodes based on randomly-oriented CNTs have been previously shown to suffer from undesirable voltage hysteresis between charging and discharging associated with the slow kinetics and poor reversibility of the Li^+ intercalation/deintercalation process. Attempts have been made to try to eliminate this problem, for example, by cutting the nanotubes to short segments to improve the charge transport capability of the electrode. Compared with a randomly-oriented CNT electrode in a conventional organic electrolyte with a potential separation of ~0.9 V between the Li^+ intercalation and deintercalation, our results clearly show a much smaller potential separation (0.35 V, inset of Figure 8b), and hence a low voltage hysteresis for the VA-CNT electrodes even in an ionic liquid electrolyte with a relatively high viscosity. Along with the high columbic efficiency, therefore, the well-defined alignment and tube spacing, enhanced electrolyte accessibility, and rapid charge transport capability intrinsically associated with the VA-CNTs have made the Li^+ intercalation/deintercalation highly reversible at the VA-CNT anode, ensuring an improved cycle life for batteries.

In order to synthesize a high-capacity and high-rate cathode to match with the high-performance VA-CNT anode necessary for developing batteries of a high-energy and high-power, we deposited V_2O_5 as a coaxial thin film around each of the individual plasma-etched VA-CNTs to produce the V_2O_5-VA-CNT composite cathode (Figure 6c). Owing to its high safety, low cost, and high theoretical capacity (590 mAh/g, corresponding to four moles of Li^+ intercalated into per mole of V_2O_5), V_2O_5 has been investigated as a potential high-performance cathode material to replace LiCoO2 for Li-ion batteries. However, the low electronic conductivity (10^{-6} ~ 10^{-7} S/cm) of and the slow Li+ diffusion (diffusion coefficient: ~ 10^{-13} cm^2/s) through V_2O_5 have severely limited its electrochemical storage application. The use of VA-CNTs with a large surface area for coaxial coating with V_2O_5 ensures a relatively large V_2O_5 loading even in a thin film form to enhance the large capacity and high rate capability for the V_2O_5-VA-CNT composite cathode (Figure 7f). The nanotube's good conductivity also facilitates the electrochemical deposition of V_2O_5 coaxially around each of the constituent CNTs in the plasma-etched VA-CNTs. The V_2O_5 loading for the V_2O_5-VA-CNT composite electrode was optimized by varying the numbers of potential cycling during the electrodeposition of V_2O_5. A low V2O5 mass loading (0.14 mg/cm^2) produced a very high capacity of 690 mAh/g (defined by V_2O_5 mass) for the composite electrode. This value of capacity is even higher than the theoretical one for pure V_2O_5 (590 mAh/g) and has been attributed to the combined energy storage arising from both the redox process of V_2O_5 and the double-layer charging of the CNT substrate. Increasing V_2O_5 loading up to 2.25 mg/cm^2 resulted in an enhanced

capacity even defined by the overall mass of the V_2O_5-VA-CNT composite. However, further increase in the V_2O_5 loading blocked the spaces between the tubes of the VA-CNTs, leading to a reduced capacity for the V_2O_5-VA-CNT composite electrode. The best deposition condition was optimized to be 80 potential cycles for the V_2O_5 electrodeposition to yield a capacity of 368 mAh/g for the resultant V_2O_5-VA-CNT composite electrode. The well-defined high surface area associated with VA-CNTs is believed to be responsible for the observed high (and efficient) V_2O_5% loading for the V_2O_5-VA-CNT composite electrode. Without blocking the intertube space (Figure 7f), the high V_2O_5% loading means a high capacity and a high rate capability for the V_2O_5-VA-CNT composite electrode.

Figure 9a shows three pairs of reversible redox peaks, attributable to the known three-step successive phase transformations on the Li^+ insertion and extraction of V_2O_5, for the V_2O_5-VA-CNT composite cathode in 1 M LiTFSI/20% EC/[EDMMEA][TFSI]. Moreover, the envelope shape of the obtained CV should be due to the capacitive behavior of the high surface area and high porosity of V_2O_5. Importantly, this indicates the proper Faradic and capacitive properties of the electrochemically synthesized V_2O_5 coaxial layer on the VA-CNT substrate in the present work. Unlike the VA-CNT anode, the V_2O_5-VA-CNT composite electrode rapidly reached its highest columbic efficiency of 99% after the first initial cycle without the formation of a SEI film (Figure 9b). During galvanostatic charging/discharging at 0.25C, the V_2O_5-VA-CNT composite electrode showed a high capacity of 368 mAh/g (Figure 9c). At a higher rate, a capacitor-like discharge behavior (linear potential decline without a plateau) was observed. At 2C, the V_2O_5-VA-CNT composite electrode retained a capacity at 230 mAh/g (capacity retention: 63 %), showing its high rate capability. Again, with respect to the relatively high viscosity and low conductivity of ionic liquids (compared to conventional electrolytes), this rate performance should be considered to be reasonably high and can be attributed to the unique porous structures of the VA-CNTs. Further charging/discharging (100 cycles) did not cause significant fading in capacity for this composite electrode, suggesting its good stability as cathode in the ionic liquid electrolyte studied.

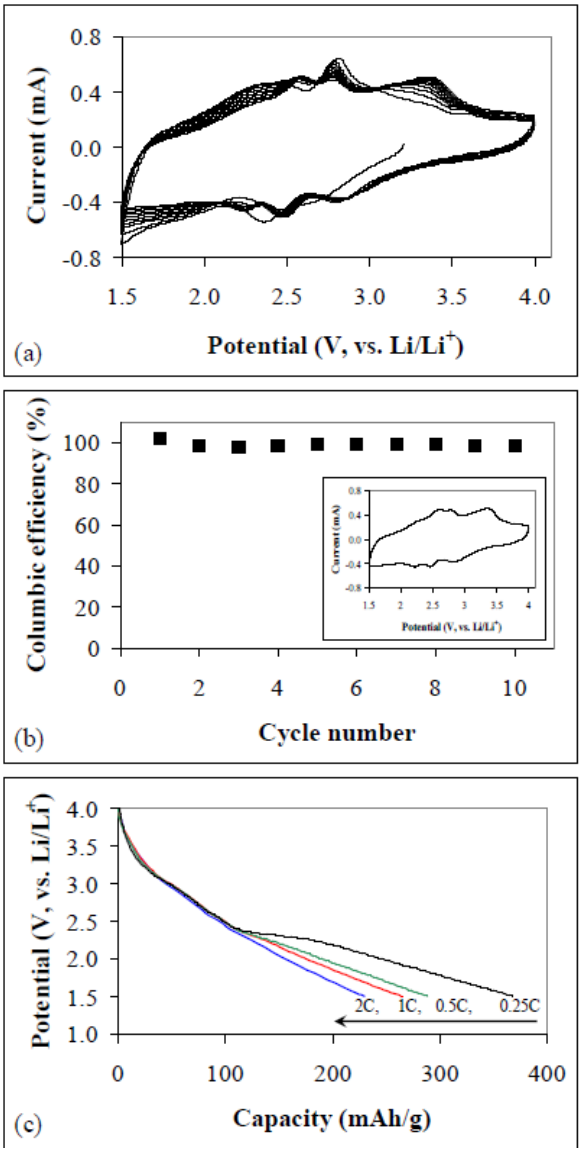

Figure 9. (a) CVs and (b) corresponding columbic efficiency of a V_2O_5-VA-CNT electrode recorded in 1 M LiTFSI/20% EC/[EDMMEA][TFSI] electrolyte. Scan rate: 1 mV/s. The inset in (b) is the 10th cycle of the CV. (c) Discharge curves of the V_2O_5-VA-CNT electrode recorded at the rates increasing from 0.25C to 2C as indicated by the arrow (curves shown were from the third cycle at each rate). Cut-off potential: 1.5 - 4 V. Galvanostatic charging/discharging (c) was performed for a same V_2O_5-VA-CNT electrode after its CV test (a). (adapted from *PhysChemChemPhys* **2012**, *14*, 12099.).

To study the performance of full battery cells, we fabricated the VA-CNT anode, the V_2O_5-VA-CNT composite cathode, and the ionic liquid electrolyte (1 M LiTFSI/20% EC/[EDMMEA][TFSI]) into prototype batteries. Due to the fact that the as-synthesized VA-CNT anode and V_2O_5-VA-CNT cathode do not contain lithium, a pretreatment is necessary to pre-lithiate one of these electrode materials prior to the assembly of a battery full cell. This can be done by electrochemically pre-lithiating either the VA-CNT anode or the V_2O_5-VA-CNT cathode. For our preliminary proof-of-concept study in the present work, we pre-lithiated the VA-CNT anode by electrochemical potential cycling. In addition to lithiation, this pretreatment can also ensure a high columbic efficiency for the VA-CNT anode prior to its use for full cell assembly. It was found that these batteries could store a large amount of energy and rapidly deliver the stored energy to achieve a high power (Figure 10). Unlike a traditional Li-ion battery where the discharge is characterized by a voltage plateau followed by a sharp voltage drop at the end of discharge, the VA-CNT based batteries developed in this study showed a supercapacitor-like linear voltage decline at a fixed rate (Figure 10a), indicating their capability to be discharged all the way down to the fully discharged state. For most conventional batteries, the achievement of a high power scarifies their energy storage capacity. This has been a long-time problem that makes the Li-ion battery technology unfavorable for high-rate applications (*e.g.*, electric vehicles). Along with recent intensive research efforts in developing Li-ion batteries with both high energy and high power [5-**Error! Reference source not found.**], we have developed the VA-CNT-based batteries to show the potential to achieve the great promise with a maximum energy density of 847 Wh/kg and a maximum power density of 35 kW/kg (Figure 10b). Based on a simplified estimation method, these active-material-based data can be converted to the corresponding values (energy density: 297 Wh/kg, power density: 12 kW/kg) for a packaged battery, possessing the potential to significantly exceed those of the current Li-ion batteries. Volumetric performance of these prototype batteries (energy density: 95 Wh/L, power density: 4 kW/L) is not as promising as their gravimetric performance, which is believed to be determined by the low packing density of VA-CNTs, a common phenomenon for nanomaterials.

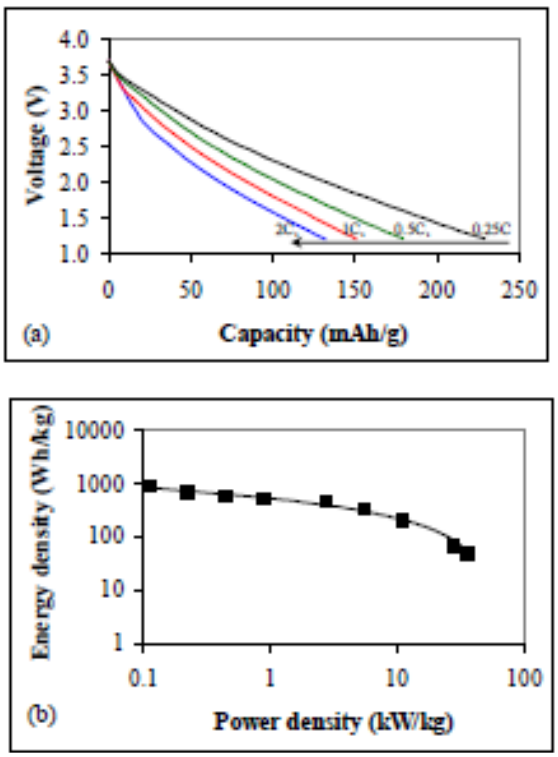

Figure 10. (a) Discharge curves of a VA-CNT/V_2O_5-VA-CNT battery recorded at the rates increasing from 0.25C to 2C as indicated by the arrow. The capacity is defined by the total active-material-mass of the anode and the cathode. Cut-off voltage: 1.2 - 3.7V. (b) Ragone plot of the VA-CNT/V_2O_5-VA-CNT battery. Performance of the battery is defined by the total active-material-mass of the VA-CNT anode and the V_2O_5-VA-CNT cathode. (adapted from *PhysChemChemPhys* **2012**, *14*, 12099.).

We have demonstrated prototype batteries with a high energy density (297 Wh/kg) and power density (12 kW/kg) (estimated from active-material-based performances) to be attractive for high-rate applications (*e.g.*, electric vehicles) - outperformed the current state-of-the-art Li-ion battery technology. The use of environmentally benign ionic liquid electrolytes can ensure a high safety and prolonged lifetime for the batteries. The present work offers a promising approach to high-performance Li-ion batteries with significantly improved energy, power, and safety. The environmental stability of V_2O_5 and CNTs will further ensure an inherently safe operation and long lifetime for these batteries.

1.7 Vertically Aligned N-Doped Coral-Like Carbon Fiber Arrays as Efficient Air Electrodes for High-Performance Non-Aqueous Li-O2 Batteries (*ACS Nano* **2014**, 8, 3015.)

Li-O_2 batteries have recently merged as high energy density devices with a theoretical energy density of ~3500 Wh kg^{-1}, nearly 8 times higher than that of commercial Li-ion batteries, and the ability to power electrical vehicles for a 500-miles range per charge. High energy efficiency and long cycleability are two important performance measures for Li-air batteries. Using a rationally designed oxygen electrode based on a vertically-aligned nitrogen-doped coral-like carbon nanofiber (VA-NCCF) array supported by stainless steel cloth, we have developed a non-aqueous Li-O_2 battery with an energy efficiency as high as 90% and a narrow voltage gap of 0.3 V between discharge/charge plateaus. To the best of our knowledge, these are the lowest overpotential and the highest energy efficiency, among the reported Li-O_2 batteries. Excellent reversibility and cycleability were also demonstrated for the newly-developed oxygen electrode. The observed outstanding performance can be attributed to its unique vertically-aligned, coral-like N-doped carbon microstructure with a high catalytic activity and an optimized oxygen/electron transportation capability, coupled with the micro-porous stainless steel substrate. These results demonstrate that highly efficient and reversible Li-O_2 batteries are feasible by using a rationally designed carbon-based oxygen electrode.

A typical non-aqueous Li-O_2 battery is composed of three essential components: 1) a metallic lithium anode, 2) a porous cathode (usually carbon based materials with or without catalysts), and 3) non-aqueous electrolyte (Li^+ containing solution) in between. The key charge/discharge reactions take place at the oxygen electrode: $2\,Li^+ + 2e + O_2 \leftrightarrow Li_2O_2$ with a thermodynamic potential of 2.96 V. During discharging, oxygen molecule is reduced by electrons from the current collector to combine with Li^+ ions dissolved in the electrolyte to produce solid Li_2O_2 on the cathode. Subsequent charging causes a reverse reaction. However, huge polarizations are commonly observed during charging, with a typical 1 ~ 2 V voltage gap between the charge and discharge plateaus. Because of the instability of non-aqueous electrolytes, the decomposition of electrolytes to form an insulate coating on the electrode surface increases the overpotential, which, in turn, accelerates the decomposition of electrolytes. So far, no stable non-aqueous electrolyte has been found. Besides, carbon materials in oxygen electrodes have been proven to decompose accompanying the electrolyte decomposition, particularly at high overpotentials. During the past several years, various approaches have been developed to address these problems and improved energy efficiencies (defined by the percentage of discharge voltage over charge voltage at the middle of the charge/discharge plateaus) from 50% to 70% for Li-O_2 batteries were achieved.

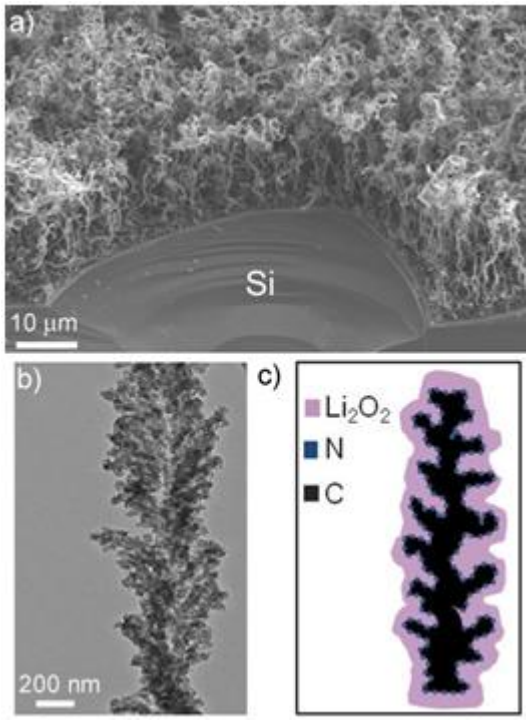

Figure 11. a) SEM image of a VA-NCCF array grown on a piece of Si wafer by CVD. b) TEM image of an individual VA-NCCF. c) The sketch of Li_2O_2 grown on a coral-like carbon fiber, which has an advantage to tightly hold the Li_2O_2 deposit by the rugged surface. (adapted from *ACS Nano* **2014**, *8*,

Generally speaking, an ideal oxygen electrode requires a highly conductive porous structure to facilitate both electron and oxygen transportations. A large specific surface area is also desirable for the electrode to show a high Li_2O_2 update. In this study, we have synthesized vertically-aligned nitrogen-doped coral-like carbon

nanofiber (VA-NCCF) arrays by chemical vapor deposition (CVD), and then transferred the resultant VA-NCCFs onto a piece of micro-porous stainless steel cloth as a binder-free oxygen electrode for non-aqueous Li-O_2 batteries. Figure 11a shows a typical SEM image for a VA-NCCF forest grown on a Si wafer with a thickness of ~20 μm and a density of ~20 μg cm^{-2}. The zigzag-like carbon fibers aligned normal to the substrate and slightly tangled with each other, leading to good conductivities for both the in-plan and through-thickness directions while providing a large free space within the layer for efficient oxygen/electrolyte transportation and a large uptake of Li_2O_2. The VA-NCCF electrode of a well-defined large surface area with all the nanofiber top-ends falling on one plane at the electrode/electrolyte interface can offer additional advantages to not only facilitate the electrolyte/reactant diffusion for current enhancement but also enhance the current transportation through the shortest pathway along the vertically-aligned fiber length without the needs of a binder. Binder-free electrode can reduce the electronic resistance, expose all active surface area to support the electrochemical process, and exclude all the possible side-effects associated with the binder decomposition. A transmission electron microscopic (TEM) image of an individual fiber is given in Figure 11b, which shows the coral-like micro-structure with many branches along the fiber "trunk" to enlarge the surface area, in respect with smooth (unbranched) carbon fibers or CNTs, for enhancing the electrode/electrolyte interaction and Li_2O_2 deposition over the whole surface of a branched fiber with a close electrical contact (*cf.* Figure 11c).

As shown in Figure 12a, a low overpotential of 0.3 V at the middle of discharge/charge plateaus was observed at the current density of 100 mA g^{-1}. The overpotentials were still reasonably low even when the current density was increased to 600 and 1000 mA g^{-1} with respect to a typical value of 1 ~ 2 V for other Li-O_2 batteries. The cut-off voltage at the end of charge was just 3.6 V at the current density as high as 1000 mA g^{-1}. To the best of our knowledge, such a low overpotential (0.3 V) was the first time reported for non-aqueous Li-O_2 batteries, which is even lower than those of noble metal based catalysts. The corresponding energy efficiency was calculated to be 90%; the highest value for non-aqueous Li-O_2 batteries reported so far. The rate performance was also investigated for a single cell started from the current density of 100 to 1500 mA g^{-1} in five sequential cycles with a controlled capacity of 1000 mAh g^{-1}. In this case, the cut-off voltage was still found to be no more than 3.8 V at the end of the fifth charge under the current density of 1500 mAg^{-1} (Figure 12a). The full capacity of the VA-NCCF electrode was explored by discharging the cell down to 2.2 V at the current density of 500 mA g^{-1}, then charging to an equivalent capacity at the same current density. A high capacity over 40000 mAh g^{-1} was demonstrated after 100 hours discharge (Figure 12b). During the subsequent charge processes, the first 10000 mAh g^{-1} capacity was made under 4.0 V and most of the rest capacity was recovered under 4.1 V. The above results clearly indicate a larger specific capacity and a smaller charging overpotential for a full discharged/charged cycle. Due to the low overpotential of the VA-

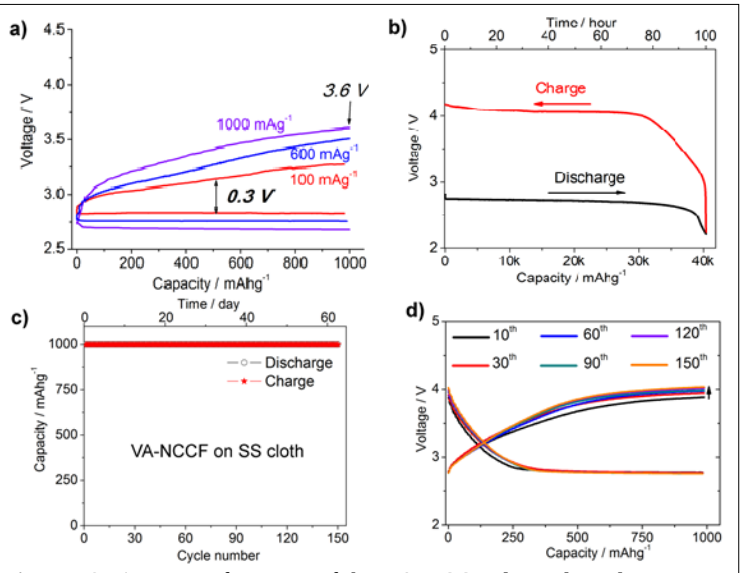

Figure 12. a) Rate performance of the VA-NCCF electrode under current densities of 100, 600 and 1000 mA g^{-1}. b) Discharge/charge voltage profile of the VA-NCCF as the function of specific capacity. The cut-off voltages were 2.2 V for discharging and 4.4 V for charging. Current density was 500 mA g^{-1}. c) Cycling performance of the VA-NCCF array on the SS cloth substrate. d) The representative discharge-charge curves from the 10^{th} to 150^{th} cycle for the VA-NCCF electrode. Current density was 500 mA g^{-1} and a controlled capacity was 1000 mAh g^{-1}. The cell has been working for more than 2 months while the testing is still continuing. (adapted from *ACS Nano* **2014**, *8*, 3015.).

NCCF electrode, the electrolyte decomposition could be minimized, leading to a long device cycle life. To investigate the stability of the VA-NCCF electrode, we performed continuous charge/discharge cycling of one cell using the SS cloth substrate for more than two months and 150 cycles at a specific capacity of 1000 mAh g^{-1} per discharge/charge cycle. As can be seen in Figures 12c&d, the cell based on the SS-supported VA-NCCF electrode showed an almost constant capacity over 150 cycles, and the voltage profile was fairly stable with little change in overpotential after the 10^{th} cycle (Figure 12d). It is the interplay of the N-doping-induced high catalytic activity, the coral-like micro-structure, and the highly conductive micro-porous SS cloth support that makes the VA-NCCF oxygen electrode to show the high energy efficiency, low overpotential, and long cycle life. This work clearly demonstrated that the performance of Li-O_2 batteries could be dramatically improved by using rationally designed oxygen electrodes with well-defined hierarchical structures and heteroatom-doping induced catalytic activities, which represents a significant advance in the research and development of Li-O_2 batteries and other energy devices.

1.8 3D N-, P-Codoped Oriented Carbon Nanofiber Frameworks as Efficeint Metal-Free Bifunctional Electrocatalysts for High-Performance Rechargeable Zn-Air Batteries (*Nat. Nanotechnol.* DOI:10.1038/nnano.2015.48, 2015.)

Rechargeable metal-air batteries have been targeted as a promising technology to meet the energy requirements for future electric vehicles and other energy-demanding devices, thanks to their high energy densities. Among the metals targeted for this type of batteries, lithium and zinc are both currently under extensive scrutiny, but Zn-air batteries have the fundamental advantage of being less costly and safer. Oxygen reduction reaction (ORR) and oxygen evolution reaction (OER) are at the heart of metal-air batteries: oxygen molecules are reduced by electrons from the current collector and combine with the metal dissolved into the electrolyte during discharging; the reverse process occurs during charging. One of the major challenges for Zn-air battery technology is to increase the O_2 reduction and evolution efficiencies, which requires the development of stable and effective bifunctional electrocatalysts possibly working in aqueous electrolytes with air as the oxygen source. Traditionally, ORR and OER are carried out with noble metals (such as Pt) and metal oxides (such as RuO_2 and MnO_2) catalysts, respectively. However, these metal-based catalysts often suffer from multiple disadvantages, including high cost, low selectivity, poor stability, and detrimental environmental effects. In this work, we show that a 3D oriented fiber-like carbon foam (Figure 13) co-doped with nitrogen and phosphorous possesses a large surface area of ~ 1663 m^2 g^{-1} and good electrocatalytic properties for both ORR and OER. This material was fabricated by a scalable, one-step process involving the pyrolysis of a polyaniline aerogel synthesized in the presence of phytic acid (Figure 13a, d). We then tested the suitability of our N, P-doped carbon foam as air

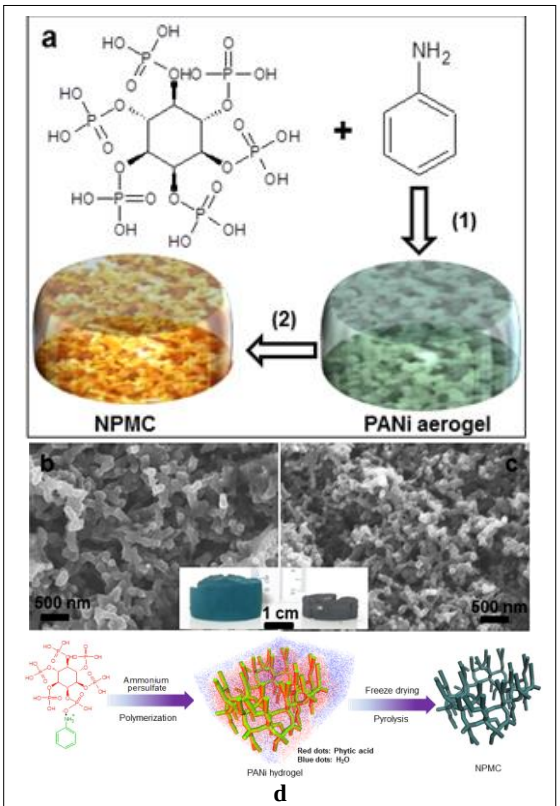

Figure 13. (a) Illustration of the preparation process of nitrogen and phosphorus co-doped porous carbon (NPMC) foams: (1) the formation of polyaniline (PANi) aerogel through an oxidative polymerization method; (2) pyrolysis of the PNAi aerogel in Ar to produce NPMC. SEM images of (b) PANi aerogel and (c) NPMC-1000. Inset is the digital picture of PANi aerogel before (*left*) and after (right) pyrolysis at 1000 °C. (d) A schematic representation of the formation process of NPMC. (adapted from *Nat. Nanotechnol.* DOI:10.1038/nnano.2015.48, 2015.).

electrodes for primary and rechargeable Zn-air batteries. Primary batteries showed an open circuit potential of 1.48 V, a specific capacity of 735 mAh g_{Zn}^{-1} (corresponding to an energy density of 835 Wh kg_{Zn}^{-1}), a peak power density of 55 mW cm^{-2}, and could sustain stable operation for 240 h after mechanical recharging. Two-electrode rechargeable batteries could be stably cycled for 180 cycles at 2 mA cm^{-2}. We also studied the activity of our carbon foam for both OER and ORR independently for air electrode operation in a three-electrode configuration and showed the ways in which the Zn-air battery can be further improved. Furthermore, our density functional theory calculations revealed that the N, P co-doping and the graphene edge effect are crucial for the bifunctional electrocatalytic activity of our material.

To test the bifunctional catalytic performance of the NPMCs, we a developed a rechargeable Zn-air battery. In a rechargeable Zn-air battery, the kinetics is mainly limited by the cathode reaction: $O_2 + 2H_2O + 4e^- \underset{OER}{\overset{ORR}{\rightleftarrows}} 4OH^-$. Figure 14a reproduces the discharge/charge cycling curves of a two-electrode rechargeable Zn-air battery that uses NPMC-1000 as a bifunctional catalyst for the air electrode, showing a good recharge-ability as evidenced by 180 discharge/charge cycles for 30 h. Although NPMC-1000 accelerates both ORR and OER, a certain degree of irreversibility is unavoidable due to the different catalytic activities of the same catalyst toward ORR and OER reactions. Consequently, a deteriorating performance was observed for the two-electrode rechargeable Zn-air battery during long-term cycling test. However, the catalytic activity of NPMC can be improved by optimizing the pore structure, heteroatom doping site, electrode surface chemistry, and cell configuration. Indeed, the NPMC battery performance was significantly enhanced by using an optimized three-electrode configuration (Figure 14b) that prevents the bifunctional catalyst to come in contact with the oxidative (or reductive) potential during ORR (or OER). In this case, the activities toward ORR and OER could be independently regulated by adjusting the catalyst mass loading on each of the two air electrodes and a balanced reversible transfer between oxygen reduction and evolution was readily achieved. Figure 14c shows the discharge and charge polarization curves for the three-electrode batteries with various air electrodes. The three-electrode rechargeable Zn-air battery using the NPMC-1000 as the air electrodes showed no obvious voltage change over 600 discharge/charge cycles (for 100 h, Figure 14d), comparable to that of three-electrode Zn-air battery using Pt/C and RuO_2 as the ORR and OER catalysts, respectively. Indeed, our battery is comparable to, or even better than, most of the recently reported rechargeable Zn-air batteries based on metal/metal oxide

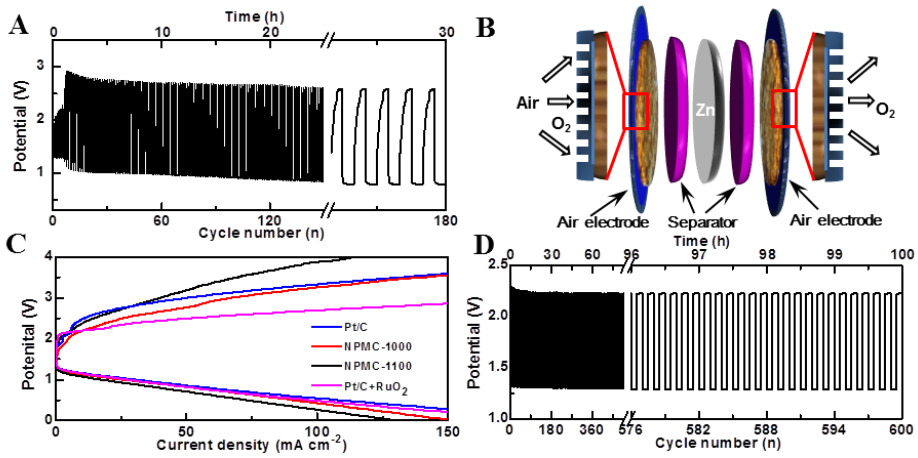

Figure 14. Performance of rechargeable Zn-air batteries. (a) Discharge/charge cycling curves of two-electrode rechargeable Zn-air batteries at a current density of 2 mA cm^{-2} using the NPMC-1000 air electrode. Three-electrode Zn-air batteries: (b) Schematic illustration for the basic configuration of a three-electrode Zn-air battery by coupling Zn electrode with two air electrodes to separate ORR and OER. The enlarged parts illustrate the porous structures of air electrodes, facilitating the gas exchange. (c) Charge and discharge polarization curves of three-electrode Zn-air batteries using the NPMC-1000, NPMC-1100, or commercial Pt/C catalyst as both of the air electrodes, along with the corresponding curve (*i.e.*, Pt/C + RuO_2) for the three-electrode Zn-air battery with Pt/C and RuO_2 nanoparticles as each of the air electrodes, respectively. (d) Discharge/charge cycling curves of a three-electrode Zn-air battery using the NPMC-1000 as the air electrodes (0.5 mg cm^{-2} for ORR and 1.5 mg cm^{-2} for OER) at a current density of 2 mA cm^{-2}. (adapted from *Nat. Nanotechnol.* DOI:10.1038/nnano.2015.48, 2015.).

electrodes. In order to gain insights into the ORR and OER catalytic mechanisms of NPMC, we performed the first-principle calculations using the density functional theory (DFT) methods, to determine the electronic structures and catalytic reactions for the N, P co-doped carbon structures. Our calculations revealed that the N, P co-doping and the graphene edge effect are crucial for the bifunctional electrocatalytic activity of our material. We expect our nanomaterial to be useful for other electrocatalytic applications as well.

1.9 Vertically-Aligned Carbon Nanotube Arrays Codoped with P and N as Efficient Metal-Free Electrocatalysts for Oxygen Reduction in Fuel Cells (*J. Phys. Chem. Lett.* 2012, *3*, 2863.)

Using a mixture of ferrocene, pyridine, and triphenyl-phosphine as precursors for injection-assisted chemical vapor deposition (CVD), we prepared the first vertically-aligned multiwalled carbon nanotube array co-doped with phosphorus (P) and nitrogen (N) with a relatively high P-doping level (designated as: PN-ACNT). We have also demonstrated the potential applications of the resultant PN-ACNTs as high-performance electrocatalysts for oxygen reduction reaction (ORR). PN-ACNT arrays were shown to exhibit a high ORR electrocatalytic activity, superb long-term durability, and good tolerance to methanol and carbon monoxide; significantly outperforming their counterparts doped with P (P-ACNT) or N (N-ACNT) only and even comparable to the commercially available Pt–C catalyst (45 wt% Pt on Vulcan XC-72R; E-TEK) due to a demonstrated synergetic effect arising from the co-doping of CNTs with both P and N (Figure 15). The superior ORR activity, together with the excellent long-term stability and good tolerance to methanol cross-over and CO poisoning effects as well as the relatively simple nanotube growth process, makes the vertically-aligned P-N co-doped MWCNT arrays ideal low-cost and high-efficient metal-free ORR catalysts for alkaline fuel cells and many other electrocatalytic reduction systems, including lithium-air batteries, DSSCs, and electrochemical biosensors.

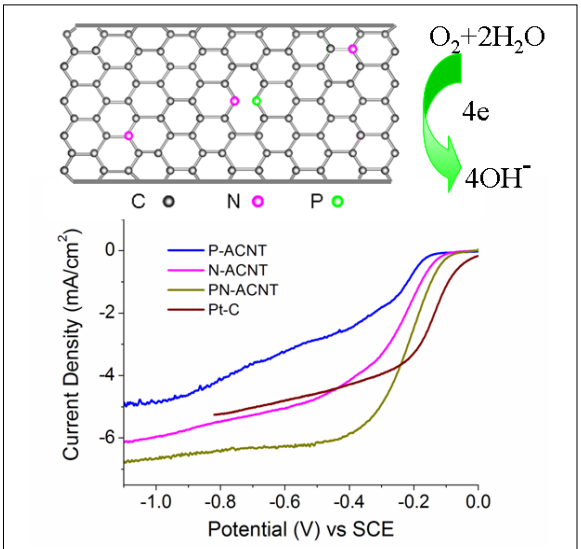

Figure 15. (*Top*) A schematic representation of the possible P-N co-doped CNT structure. (*Bottom*) RDE voltammograms of the P-ACNT/GC, N-ACNT/GC, PN-ACNT/GC, and Pt-C/GC electrodes in an oxygen-saturated, 0.10 M KOH solution at a rotation rate of 1600 rpm. Scan rate: 10 mV s −1. (adapted from *J. Phys. Chem. Lett.* 2012, *3*, 2863.).

2. SUMMARY OF ACCOMPLISHMENTS ON CONTROLLED SYNTHESIS AND FUNCTIONALIZATION OF VERTICALLY-ALIGNED CARBON NANOTUBES FOR BIO-RELATED APPLICATIONS

2.1 Platinized Aligned Carbon Nanotube-Sheathed Carbon Fiber Microelectrodes for In Vivo Amperometric Monitoring of Oxygen (*Anal. Chem.* **2014**, *86*, 5017.)

As a common electron acceptor of over one hundred known enzymes, for example, O_2 is involved in many biochemical reactions to generate energy in vivo, including adenosine triphosphate (ATP) metabolism. On the other hand, O_2 is also involved in the synthesis, metabolism, release and uptake of neurotransmitters. Under ischemia conditions, the decrease of cerebral blood flow (*i.e.*, lower availability of O_2) has been reported to disturb these processes, even leading to death and disability.

As an essential element in neural injury and brain dysfunction during ischemia, O_2 plays critical roles in the complicated neurochemical processes. Thus, *in vivo* monitoring of O_2 fluctuation during brain ischemia could offer a straightforward approach to better understanding of neurochemical processes involved in brain ischemia. In this study, we developed a new electrochemical method for selectively monitoring O_2 in vivo using platinized vertically-aligned carbon nanotube (VACNT)-sheathed carbon fibers (Pt/VACNT-CFs) as electrodes. The VACNT-sheathed CFs (VACNT-CFs) were produced via pyrolysis of iron phthalocyanine (FePc) on the surface of CFs, followed by electrochemical deposition of platinum nanoparticles to form Pt/VACNT-CFs. The resulting Pt/VACNT-CF microelectrodes exhibited fast electron transfer kinetics for O_2 reduction via a four-electron process free from the toxic H_2O_2 intermediate. Consequently, effective and selective electrochemical sensors were developed from the Pt/VACNT-CF microelectrodes for reliable measurements of O_2 in rat brain even in the presence of some interference species, such as dopamine, uric acid, 5-hydroxytryptamine, and H_2O_2, and the O_2 fluctuation in hippocampus during global cerebral ischemia/reperfusion.

Figure 16 displays SEM images of the VACNT-CF (A), Pt/CF (B) and Pt/VACNT-CF (C). Compared with the smooth surface of CF (o.d. 7 μm) (data not shown), a cross-section-view SEM image of the VACNT-CF taken after deliberately disturbing aligned CNTs along its length (Figure 10A) shows that VACNTs of ca. 3 μm length were densely packed on the CF surface to form a coaxial VACNT-CF microelectrode (o.d. ca. 13 μm). The VACNTs well-aligned around a CF can maintain a good porosity with a large surface area and excellent electrochemical properties, with the CF support providing mechanical stability and efficient electrical conduction to/from the VACNTs. Inspection of VACNT after Pt deposition clearly shows that many densely packed Pt nanoparticles homogenously distribute on the surface of VACNTs (Figure 10C). Although Pt nanoparticles could also be electrochemically deposited onto the pristine CFs under the same conditions, the resulting Pt particles distribute on the CFs more loosely (Figure 16B). This difference in morphologies of the Pt nanostructures electrodeposited on the CF and VACNT-CF is attributed to different electronic and porous properties of the CNT and CF. Moreover, cyclic voltammograms (CV) obtained on the Pt/VACNT-CF in acidic media exhibits adsorption and desorption of hydrogen in the range from -0.2 V to 0.1 V (Figure 16D), characteristic of clean electroactive surface of Pt.

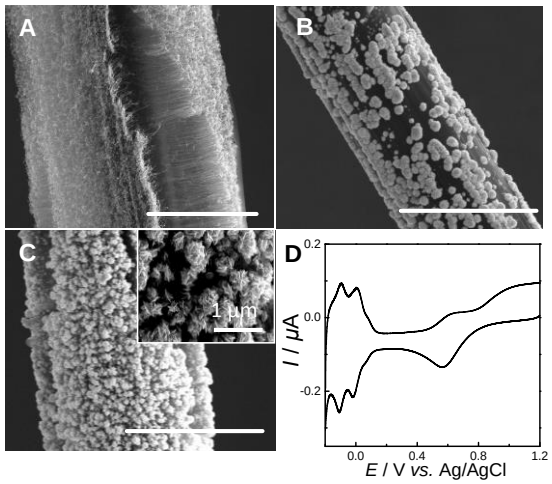

Figure 16. SEM images of the VACNT-CF (A), Pt-CF (B) and Pt/VACNT-CF (C). Scale bar, 10 μm (A, B, and C). Inset in (C) shows that many densely packed Pt nanoparticles homogenously distribute on the surface of VACNTs (D) Typical cyclic voltammogram (CV) obtained from the Pt/VACNT-CF in 0.5 M H_2SO_4 solution. Scan rate, 100 mV s^{-1}. (adapted from *Anal. Chem.* **2014**, *86*, 5017.).

Figure 17 compared the reduction process of O_2 at the bare CF (A), VACNT-CF (B), Pt/CF(C) and Pt/VACNT-CF (D) microelectrodes. On the bare CF microelecctrode, O_2 was electrochemical reduced with large overpotential (-0.8 V *vs.* Ag/AgCl), indicating a sluggish electron transfer process. Clearly, the VACNT-CF exhibited a more positive onset potential and much larger reduction current (Figure 17B), indicating a much faster electron transfer kinetics for O_2 reduction reaction on the VACNT-CF than on a bare CF. This fast electron transfer is commonly observed for O_2 reduction reaction at CNTs-based electrode *via* an overall two-electron step to form the H_2O_2 intermediate, which is very toxic to brain tissues. Interestingly, the onset potential of O_2 reduction reaction on the Pt/VACNT-CF occured at 0.1 V (Figure 17D), which is about 0.25 V and about 0.05

V more positive than those on the VACNT-CF (Figure 17B) and Pt/CF (Figure 17C), respectively. In addition, we found that the steady-state reduction current at Pt/VACNT-CF (0.37 μA) is almost twice of that at the VACNT-CF (0.16 μA) and Pt/CF (0.2 μA). The close onset potential to that of the Pt/CF, along with a higher steady-state reduction current than that of the Pt/CF, observed for the Pt/VACNT-CF indirectly indicates a four-electron O_2 reductive process at the platinized VACNT-CF electrode. The Pt/VACNT-CF electrode of the demonstrated good electrocatalytic properties would offer an opportunity for in vivo O_2 detection in ischemia process. The excellent electrochemical properties of the Pt/VACNT-CF microelectrode make it possible for selective detection of O_2 even with other electroactive species coexisting in the cerebral systems. As shown in Figure 18A, the presence of other electrochemically active species at their physiological levels in the central nervous system, including 40 μM AA, 1 μM DA, 20 μM DOPAC, 50 μM UA, 10 μM 5-HT and 1.0 μM H_2O_2, did not produce any observable current response when the electrode was poised at -0.5 V, suggesting that these species do not interfere with the monitoring of O_2. It is well known that reduction of H_2O_2 can also be electrocatalyzed on Pt surface at the similar potential with O_2 reduction, thus H_2O_2 is the most potential interference for the O_2 measurement, and hence H_2O_2 requires special attention. However, H_2O_2 (1 μM) at the physiological level was demonstrated to display minimal response compared with that of the physiological level of O_2 (30-80 μM). These results ascertain the high selectivity for O_2 measurements with the Pt/VACNT-CF microelectrode, and further ensure our newly-developed analytical approach for selective measurements of O_2 in the rat brain. In addition to the high selectivity toward O_2, the Pt/VACNT-CF microelectrode also showed a good linearity for the measurement of O_2. As can be seen in Figure 18B, the steady-state currents increased proportionally in three standard solutions (N_2-purged, air-saturated, and O_2-saturated aCSF) at the as-prepared Pt/VACNT-CF microelectrode (I / nA = 0.91C_{O2}(μM) + 40.89, γ = 0.9951). We have also investigated the reproducibility of the Pt/VACNT-CF microelectrodes by comparing the current responses to O_2 on different microelectrodes. We found that, for all of the Pt/VACNT-CF microelectrodes, a well-defined sigmoid-shaped voltammogram was obtained for the O_2 reduction with almost the same current response, suggesting that the Pt/VACNT-CF microelectrodes could be easily and reproducibly fabricated by our method. The unique electrochemical property of the Pt/VACNT-CF microelectrodes, together with their demonstrated selectivity, stability and linearity, makes the Pt/VACNTs-CF particularly attractive for in vivo monitoring of O_2.

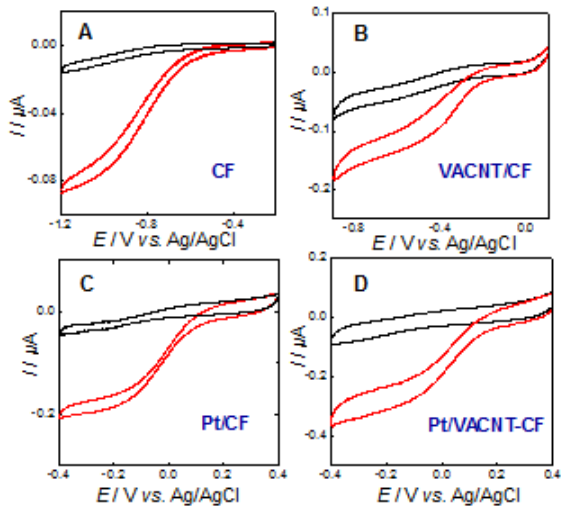

Figure 17. Typical CVs at the bare (A) CF, (B) VACNT-CF, (C) Pt/CF and (D) Pt/VACNT-CF microelectrode in aCSF (pH 7.4) saturated with N_2 (black curve) or ambient air (red curve). Scan rate, 50 mV s^{-1}. (adapted from *Anal. Chem.* **2014**, *86*, 5017.).

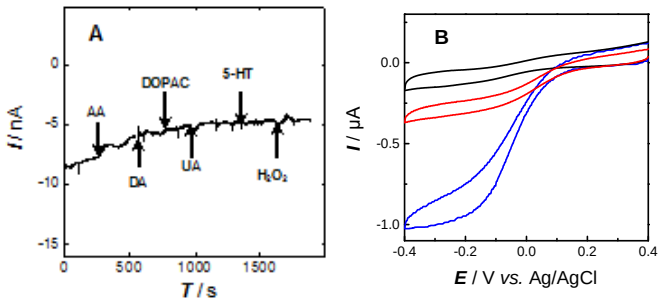

Figure 18. (A) Typical amperometric response of 40 μM AA, 1 μM DA, 20 μM DOPAC, 50 μM UA, 10 μM 5-HT, and 1.0 μM H_2O_2 at the Pt/VACNT-CF. The electrode was poised at -0.5 V *vs.* Ag/AgCl (aCSF). (B) Typical CVs at the Pt/VACNT-CF microelectrode in aCSF (pH 7.4) saturated with N_2 (blank curve), ambient air (red curve), or O_2 (blue curve). Scan rate, 50 mV s^{-1}. (adapted from *Anal. Chem.* **2014**, *86*, 5017.).

Figure 19 shows a typical dynamic current response curve recorded with the Nafion-coated Pt/VACNT-CF microelectrode at -0.50 V in the rat hippocampus during global ischemia/reperfusion. As seen in Figure 13, when the animal was administrated with global ischemia by occluding the bilateral common carotid arteries, the extracellular O_2 was quickly decreased to a low level (1.6 ± 0.1 μM, n = 3). This level was gradually restored to basal level after reperfusion, indicating a return to normal conditions. More interestingly, at the very beginning of reperfusion, O_2 current even transiently abounds to exceed pre-ischemia levels, indicating the existence of post-ischemic hyper-perfusion that has long been documented in animal stroke models or a low O_2 consumption at the early stage of reperfusion because of some cell are damaged. These results suggest that the Pt/VACNT-CF microelectrode can be used for effectively monitoring O_2 in the brain during ischemia to facilitate future studies on the neurochemical processes involved in various physiological events. Thus, this study offers a novel and reliable strategy for making new microelectrodes for in vivo monitoring of O_2 in various physiological processes with a high sensitivity, electivity, and reliability.

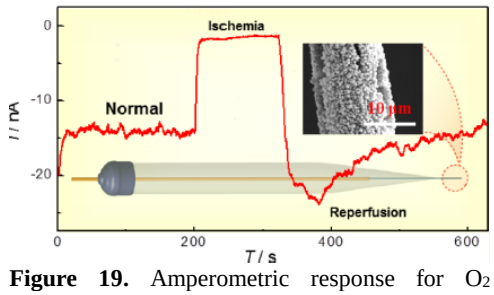

Figure 19. Amperometric response for O_2 recorded in vivo during global ischemia/reperfusion with the Nafion-coated Pt/VACNT-CF microelectrode implanted into hippocampus as the working electrode polarized at -0.5 V *vs.* Ag/AgCl (aCSF). (adapted from *Anal. Chem.* **2014**, *86*, 5017.).

2.2 Smart Gecko-Foot-Mimetic VA-CNT Wet and Dry Adhesives (*to be published*)

By using VA-CNT arrays with a straight body segment and a curly entangled top, we have previously created gecko-foot–mimetic dry adhesives that show macroscopic strong adhesive forces. In this study, we have synthesized a novel wet adhesive copolymer by preparing N-(3,4-dihydroxyphenethyl) methacrylamide (Figure 20A), followed by incorporating the dopamine-containing monomers into a PDMS copolymer and VA-CNT array (Figure 20B).

As shown in Figure 20 (C, D), the resultant flexible and sticky dry and wet adhesives exhibited both dry and wet adhesion forces with a record high wet adhesion (in water) 12.4 N/cm^2 and an excellent repeatability.

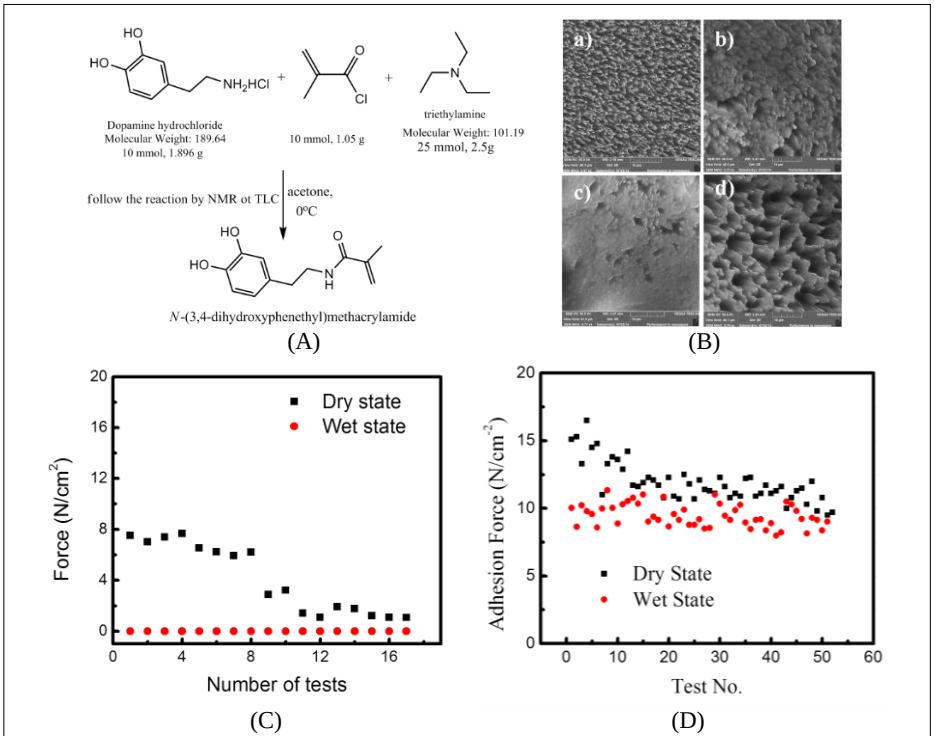

Figure 20. (A) The process to prepare N-(3,4-dihydroxyphenethyl) methacrylamide. (B) SEM images of the copolymer embedded VA-CNT array: a) before the heat treatment (60°C), b-c) under a heat treatment at 60°C, and d) after heat treatment was totally released. Repeated adhesion tests for: (C) The pristine VA-CNT array. (D) The VA-CNT array infiltrated with the dopamine-containing polymer in 60°C water (Note: the preloading force of the pristine VA-CNT array test is 0.3 MPa, and 0.03MPa for other tests).

2.2 Smart Gecko-Foot-Mimetic VA-CNT Adhesives for High-Temperature and Rough Surface (*to be published*)

Adhesion failures at extreme temperatures could cause catastrophes. For high-temperature applications (*e.g.*, >500ºC), ceramic adhesives and/or metal welding are normally considered since they can stand up to temperatures even over 1000ºC. However, interfacial debonding cannot be prevented due to the differential thermal expansions between the adhesive "layer" and target surfaces, especially over thermal transitions with a wide temperature range. In this study, we developed a class of rationally-designed vertically-aligned carbon nanotube (CNT) dry adhesives with plasma-induced top nodes, which showed a temperature-enhanced adhesion force up to 143 N/cm^2 against rough surfaces over hundreds temperature cycles from -196 to 1000˚C. This work represents a breakthrough in designing CNT and many other dry adhesives of strong adhesion forces with rough surfaces for various practical applications over wide temperature ranges.

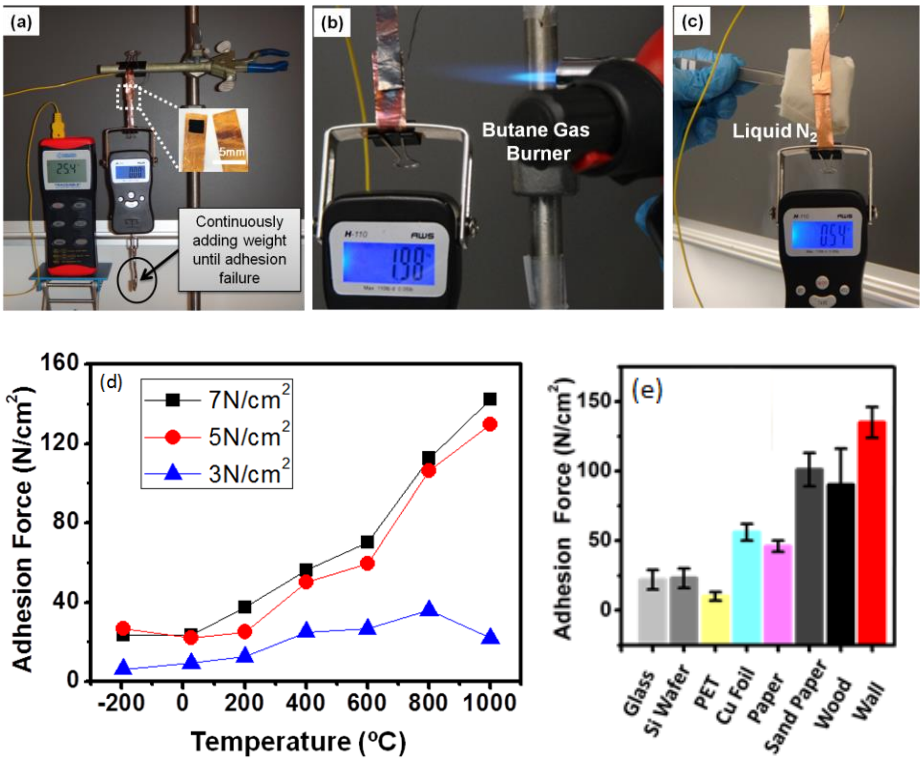

Figure 21. Set-up for dry adhesion measurements. (a) 25.4°C. (b) 1033°C. (c) -190.7°C (d) Temperature dependence of adhesion forces of the VA-CNT array from -196 to 1000°C measured under a preloading force of 3 N/cm^2, 5 N/cm^2 and 7 N/cm^2, respectively. (e) Adhesion forces of the VA-CNT array dry adhesives aganist various naturally rough surfaces, including metal foils, polymers, wood pieces, paper sheets, and even painted walls, with the adhesion force ranging from 37 to 137 N/cm^2 at ambinet temperature.

3. SUMMARY OF ACCOMPLISHMENTS ON OTHER ENERGY RELATED APPLICATIONS

3.1 Graphene Oxide-Based Carbon Interconnecting Layer for High-Performance Polymer Tandem Solar Cells (*Nano Lett*. **2014**, *14*, 1467.)

Tandem polymer solar cells (PSCs), consisting of more than one (normally two) subcells connected by a charge recombination layer (i.e., interconnecting layer), hold great promise for enhancing the performance of PSCs. For an ideal tandem solar cell, the open circuit voltage (V_{oc}) equals to the sum of those of the subcells while

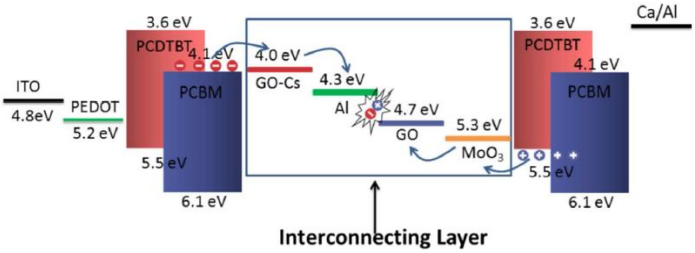

Figure 22. Schematic energy-level diagram for the various layers of the optimized tandem device.. (adapted from *Nano Lett*. **2014**. *14*. 1467.).

keeping the short circuit current the same as the lower one, leading to an increased overall power conversion efficiency. The interconnecting layer plays an important role in regulating the tandem device performance. Here, we report that graphene oxide (GO)/GO-Cs (cesium neutralized GO) bilayer modified with ultrathin Al and MoO_3 can act as an efficient interconnecting layer in tandem PSCs to achieve a significantly increased V_{oc}, reaching almost 100% of the sum of the subcell V_{ocs} under standard AM 1.5 conditions.

3.2 Graphene Oxide Derivatives as Charge Extraction Materials for High-Performance Bulk Heterojunction Solar Cells (*Adv. Mater.* **2012**, *24*, 2227.)

The intensive ongoing research into polymeric solar cells could provide the world with very cost-efficient and clean energy from sunlight. However, the energy conversion efficiency of polymer solar cells is still not high enough for practical deployment. The energy barriers between the active layer and electrodes in a polymer solar cell can be reduced by electron-/hole-extraction layers near to the cathode/anode to enhance the device performance. In this study, we demonstrated that graphene oxide with carboxylic edge-groups derived from acidic oxidation of graphene (a one-atomic sheet of carbon) can act as an efficient hole-extraction layer. By simple neutralization of the acidic graphene oxide with Cs_2CO_3, we found that the resulting Cesium-neutralized graphene oxide is an excellent electron-extraction layer. The newly-developed single hole-/electron-extraction material system could not only outperform the existing hole- and electron-extraction layers but also simplify the materials design and device fabrication with a precisely controlled energy barrier for electron- and hole-extraction.

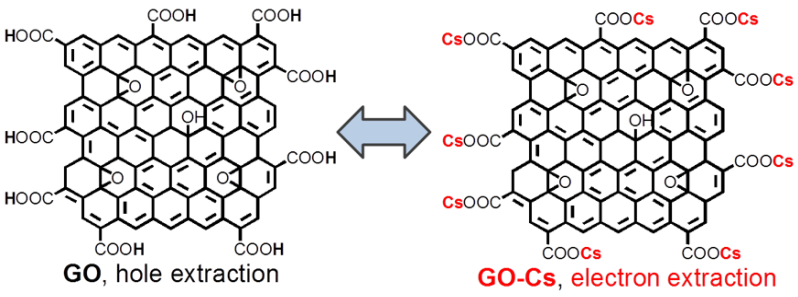

Figure 22. Charge neutralization of carboxylic acid groups in GO with Cs_2CO_3 to afford GO-Cs as electron extraction material. (adapted from *Adv. Mater.* **2012**, *24*, 2227.).

3.3 Edge-Selectively Halogenated Graphene Nanoplatelets (XGnPs, X = Cl, Br, or I) Prepared by Ball-Milling and Used as Anode Materials for Lithium-Ion Batteries (*Adv. Mater.* **2014**, *26*, 7317.)

By simply ball-milling graphite with chlorine (Cl_2), bromine (Br_2) or iodine (I_2), for instance, we have successfully prepared a series of edge-selectively halogenated graphene nanoplatelets (XGnPs, X = Cl, Br or I). These edge-functionalized GnPs (EFGnPs) were employed as promising metal-free electrocatalysts for oxygen reduction reaction (ORR) in fuel cells. The XGnPs displayed excellent electrocatalytic activities with good cycle stability. Compared with other approaches for production of graphene, including chemical vapor deposition (CVD), arc-discharge, Hummer's methods, and solvothermal synthesis, this simple, eco-friendly ball-milling method is a low-cost and scalable approach for production of XGnPs as anode materials to meet the ever-increasing demand of LIBs for our near-term needs, for example in a wide range of electric vehicles. In this study, we used edge-selectively halogenated GnPs (XGnPs, X = Cl, Br, or I) prepared by the ball-milling method as anode materials for lithium-ion batteries (LIBs). For comparison, edge-hydrogenated GnP (HGnP) was also prepared by ball-milling graphite in the presence of hydrogen. This method employed the

repulsive interaction of edge- halogenated groups as the driving force to gradually exfoliate the graphite into XGnPs during the ball-milling process, and thus allowed for a low-cost and large-scale production of XGnPs. It was found that IGnP electrode delivered an initial charge capacity of 562.8 mAh g^{-1} at 0.5 C in the voltage range of 0.02 - 3.0 V, which was higher than the reference HGnP with 511.3 mAh g^{-1}. Furthermore, after 500 cycles, the IGnP electrode was still able to deliver a higher charge capacity of 458.0 mAh g^{-1} with a higher initial charge capacity retention of 81.4% than the HGnP with 208.5 mAh g^{-1} and 40.8%, respectively. After 500 cycles and 1 month storage at ambient condition (25 °C), the IGnP cell still maintained a reversible capacity of 464.1 mAh g^{-1} at the end of additional 100 cycles, indicating a remarkably high stability. Such excellent electrochemical performance of the IGnP as anode for LIBs is attributable to the high electronegativity of I (χ = 2.66 higher than χ = 2.55 for carbon), high surface area of IGnP (736.8 m^2 g^{-1}), as well as the improved lithium-ion insertion/extraction at the edges ($d_I > d_H$) between graphitic layers, which should lead to enhanced lithium-ion transportation through the electrolyte and electrode during cycling.

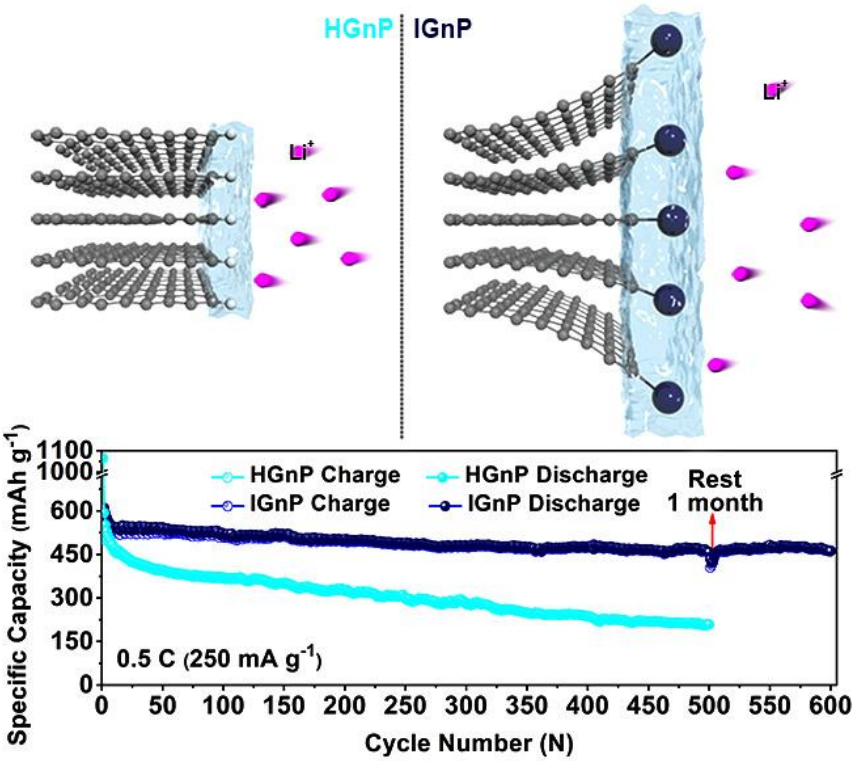

Figure 23. (*Top*) A schematication presentation for the edge expansion for the HGnP and IGnPs caused by edge groups ($d_I > d_H$). (*Bottom*) Cycling performance at 0.5 C of HGnP and IGnPs, the continued cycling performance of the IGnP cell was obtained after 500 cycles and 1 month storage at ambient condition (25 °C). (adapted from *Adv. Mater.* **2014**, *26*, 7317.).

3.4 Well-Defined Two Dimensional Covalent Organic Polymers: Rational Design, Controlled Syntheses, and Potential Applications (*Polym. Chem.* **2015**, *6*, 1896.)

Two-dimensional (2D) covalent organic polymers (COPs) and derivatives hold great potential for a large variety of applications, including gas storage, sensing, energy conversion and storage, and electrocatalysis. Moreover, 2D COPs offer excellent opportunities for fundamental study on an exciting class of new polymeric materials with unique 2D structures and novel properties. However, the design and synthesis of well-defined 2D COPs remain a big challenge. In this invited article, we review recent progresses on 2D COPs and derivatives. Some concepts on the rational design and syntheses of well-defined 2D COPs and derivatives will be discussed, along with their potential application as well as perspectives and challenges in this emerging field.

Figure 24. Cover of *Polym. Chem.* **2015**, *6*, 1896.).

3.5 Nitrogen enriched porous carbon spheres: Attractive materials for supercapacitor electrodes and CO2 adsorption (*Chem. Mater.* **2014**, *26*, 2820.)

A series of nitrogen-containing polymer and carbon spheres were obtained by a sol-gel method. In particular, the nitrogen-rich carbon spheres were prepared by one-pot hydrothermal synthesis in the presence of resorcinol/formaldehyde as carbon precursors and ethylenediamine (EDA) as both a base catalyst and nitrogen precursor, followed by carbonization in nitrogen and activation with CO_2. The introduction of EDA to the sol-gel system resulted in structurally bonded nitrogen-containing carbon spheres. The nitrogen doping level and the particle size can be tuned by varying the EDA amount in the reaction mixture. The maximum nitrogen doping level of 7.2 wt % in carbon spheres could be achieved without sacrificing the spherical morphology. The diameter of these carbon spheres can be tuned in the range of 50-1200 nm by varying the EDA amount. N_2 adsorption analysis showed that the aforementioned activated carbon spheres exhibited a high surface area up to 1224 m^2/g. Ultra high CO_2 adsorption capacities, 4.1 and 6.2 mmol/g, were measured on the nitrogen-containing activated carbon spheres at 1 bar and 25 and 0 ºC, respectively. Electrochemical measurements performed on these carbon spheres for double layer capacitors showed very a high capacitance up to ~388 F/g at 1.0 A/g, outstanding rate capability (60 % capacitance retention at 100 A/g) and unprecedented cycling stability (~98 % capacitance retention even after 8000 cycles) in 1 M H_2SO_4 electrolyte solution.

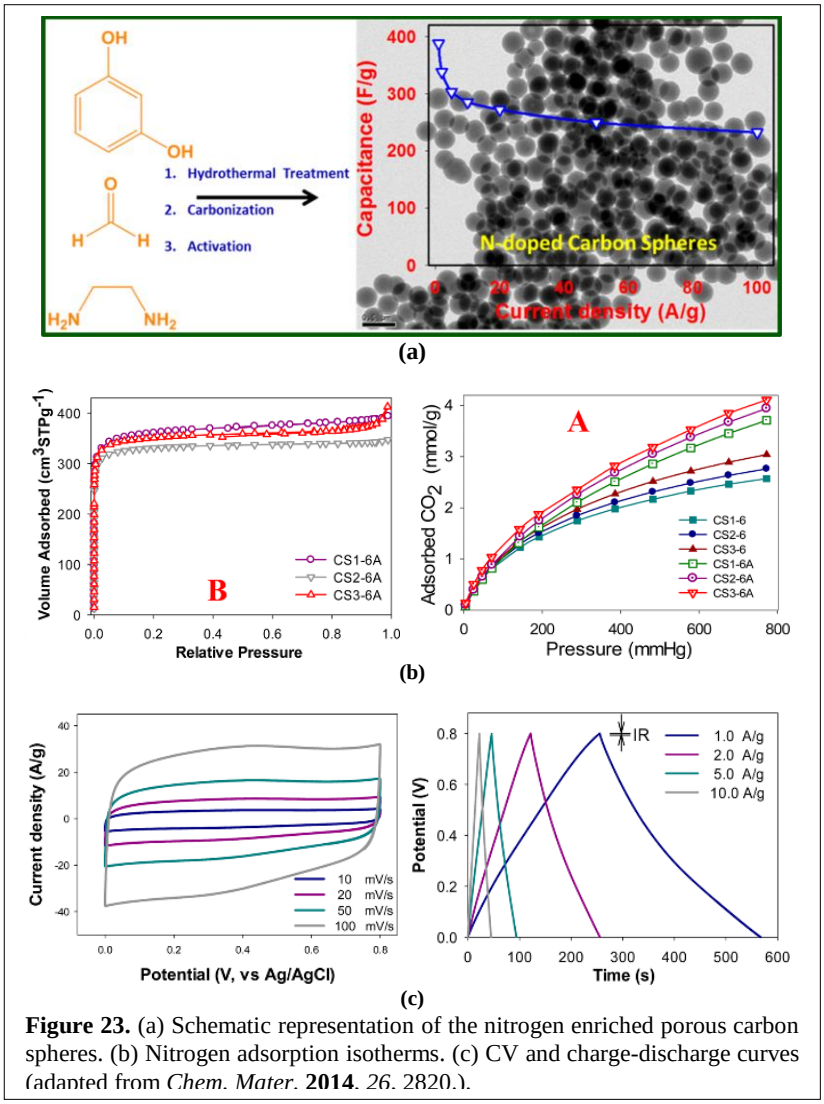

Figure 23. (a) Schematic representation of the nitrogen enriched porous carbon spheres. (b) Nitrogen adsorption isotherms. (c) CV and charge-discharge curves (adapted from *Chem. Mater.* **2014**, *26*, 2820.).

II. JOURNAL PAPERS PUBLISHED FROM THIS PROJECT WITH ACKNOWLEDGEMENTS TO THE AFOSR GRANT AND BOOK CHAPTERS

JOURNAL PUBLICATIONS

1. J. Zhang, Z. Zhao, Z. Xia, L. Dai. "A metal-free bifunctional electrocatalyst for oxygen reduction and oxygen evolution reactions"
   Nat Nanotechnol. DOI:10.1038/nnano.2015.48, 2015.
2. L. Dai, Y. Xua, L. Qu, H.-J. Choi, J.-B. Baek. "Metal-Free Catalysts for Oxygen Reduction Reaction"
   Chem. Rev. 2015, DOI: 10.1021/cr5003563.
3. T. Chen, R. Hao, H. Peng, L. Dai. "High-performance, extremely stretchable, wire-shaped supercapacitors"
   Angew. Chem. Int. Ed. 54, 618–622, 2015.
4. J. Xu, M. Wang, N. P. Wickramaratne, M. Jaroniec, S. Dou, L. Dai. "High-Performance Sodium Ion Batteries Based on Three-Dimensional Anode from Nitrogen-Doped Graphene Foams"
   Adv. Mater .27, 2042-2048, 2015.
5. Z. Xiang, D. Cao, L. Dai. "Well-Defined Two Dimensional Covalent Organic Polymers: Rational Design, Controlled Syntheses, and Potential Applications"
   Polym. Chem. 6, 1896-1911, 2015.
6. I.-Y. Jeon, M.J. Ju, J. Xu, H.-J. Choi, J.-M. Seo, M.-J. Kim, I. T. Choi, H.M. Kim, J.C. Kim, J.-J. Lee, H. K. Liu, H.K. Kim, S. Dou, L. Dai, J.-B. Baek. "Edge-Fluorinated Graphene Nanoplatelets as High Performance Electrodes for Dye-Sensitized Solar Cells and Lithium Ion Batteries"
   Adv. Funct. Mater. 25, 1170-1179, 2015.
7. Y. Xue, J.M. Baek, H. Chen, J. Qu, L. Dai. "N-doped graphene nanoribbons as efficient metal-free counter electrode for disulfide/thiolate redox mediated DSSCs"
   Nanoscale 7, 7078-7083, 2015.
8. Y. Xue, L. Zhu, H. Chen, J. Qu, L. Dai. "Multiscale patterning of graphene oxide and reduced graphene oxide for flexible supercapacitors" *Carbon* (2015) DOI: org/10.1016/j.carbon.2015.04.046.
9. J. Liu, M. Durstock, L. Dai. "Graphene oxide derivatives as hole- and electron- extraction layers for high-performance polymer solar cells"
   Energy Environ. Sci. 7, 1297-1306, 2014.
10. D. Yu, K. Goh, H. Wang, L. Wei, W. Jiang, Q. Zhang, L. Dai, Y.Chen. "Scalable synthesis of hierarchically-structured carbon nanotube-graphene fibres for capacitive energy storage"
    Nat. Nanotechnol. 9, 555–562, 2014.
11. T. Chen, H. Peng, M. Durstock, L. Dai. "High-performance transparent and stretchable all-solid supercapacitors based on highly aligned carbon nanotube sheets"
    Sci. Rep., 4, 3612, 2014.
12. Y. Chen, W.-C. Lin, J. Liu, L. Dai. "Graphene oxide-based carbon interconnecting layer for high-performance polymer tandem solar cells"
    Nano Lett., 14 (3), 1467–1471, 2014.
13. J. Xu, I.-Y. Jeon, J.M. Seo, S. Dou, L. Dai, J.-B Baek. "Edge-selectively halogenated graphene nanoplatelets (XGnPs, X = Cl, Br, or I) prepared by ball-milling and used as anode materials for lithium-ion batteries"
    Adv. Mater. 26, 7317–7323, 2014.
14. N. P. Wickramaratne, J. Xu, M. Wang, L. Zhu, L. Dai, M. Jaroniec. "Nitrogen enriched porous carbon spheres: Attractive materials for supercapacitor electrodes and CO2

adsorption"
Chem. Mater. 26, 2820−2828, 2014.
15. J. Xu, J. Shui, J. Wang, M. Wang, H.-K. Liu, S.X. Dou, I.-Y. Jeon, J.-M. Seo, J.-B. Baek, L. Dai. "Sulfur-graphene nanostructured cathodes via ball-milling for high-performance lithium-sulfur batteries"
ACS Nano 8, 10920-10930, 2014.
16. D. Wang, J. Chen, L. Dai. "Recent advances in graphene quantum dots for fluorescence bioimaging from cells through tissues to animals"
Particle & Particle Systems Characterization, DOI:10.1002/ppsc.201400219, 2014.
17. J. Liu, M. Durstock, L. Dai. "Graphene oxide derivatives as hole- and electron- extraction layers for high-performance polymer solar cells"
Energy & Environmental Science 7, 1297-1306, 2014.
18. J. Shui, F. Du, C. Xue, Q. Li, L. Dai, "Vertically aligned N-doped coral-like carbon fiber arrays as efficient air electrodes for high-performance non-aqueous Li-O_2 batteries"
ACS Nano 8 (3), 3015–3022, 2014.
19. T. Chen, L. Dai, "Flexible supercapacitors based on carbon nanomaterials"
J. Mater. Chem. A, 2, 10756-10775, 2014.
20. L. Xiang, P. Yu, Y. Wang, M. Zhang, L. Zhu, L. Dai, L. Mao. "Platinized aligned carbon nanotube-sheathed carbon fiber microelectrodes for in vivo amperometric monitoring of oxygen"
Anal. Chem. 86, 5017-5023, 2014.
21. L. Dai. "Functionalization of graphene for efficient energy conversion and storage"
Acc. Chem. Res. 46, 31-42, 2013.
22. W. Lu, L. Dai. "Carbon nanotubes for advanced energy conversion and storage"
J. Nano Energy Power Res. 2, 1-24, 2013.
23. I.-Y. Jeon, H.-J. Choi, M. J. Ju, I. T. Choi, K. Lim, J. Ko, H. K. Kim, J. C. Kim, J. J. Lee, D. Shin, S.-M. Jung, J.-M. Seo, M.-J. Kim, N. Park,L. Dai, J.-B. Baek. "Direct nitrogen fixation at the edges of graphene nanoplatelets as efficient metal-free electrocatalysts for energy conversion"
Scientific Reports 3, 2260, 2013.
24. T. Chen, L. Dai. "Carbon nanomaterials for high-performance supercapacitors"
Materials Today 16, 272-280, 2013.
25. J. Liu, Y. Xue, M. Zhang, L. Dai. "Graphene-based materials for energy applications"
MRS Bull. 37, 1265-1272, 2013.
26. I.-Y. Jeon, H.-J. Choi, M. Choi, J.-M. Seo, S.-M. Jung, M.-J. Kim, S. Zhang, L. Zhang, Z. Xia, L. Dai, N. Park, J.-B. Baek. "Facile, scalable synthesis of edge-halogenated graphene nanoplatelets as efficient metal-free eletrocatalysts for oxygen reduction reaction"
Scientific Reports 3, 1810, 2013.
27. Y. Xue, D. Yu, L. Dai, R. Wang, D. Li, A. Roy, F. Lu, H. Chen, Y. Liu, J. Qu."Three-dimensional B, N-doped graphene foam as metal-free catalysts for oxygen reduction reaction"
Phys.Chem.Chem. Phys. 15, 12220-12226, 2013.
28. J. Xu, S. Dou, H. Liu, L. Dai. "Cathode materials for next generation lithium ion batteries"
Nano Energy 439-442, 2013.
29. I.-Y. Jeon, Y.-R. Shin, G.-J. Sohn, H.-J. Choi, S.-Y. Bae, J. Mahmood, S.-M. Jung, J.-M. Seo, M.-J. Kima, D. W. Chang, L. Dai, and J.-B. Baek. "Edge-carboxylated graphene nanosheets via ball milling"
Proc. Natl. Acad. Sci. USA 109, 5588-5593, 2012.
30. Y. Xue, J. Liu, H. Chen, R. Wang, D. Li, J. Qu, L. Dai. "Nitrogen-doped graphene foams as metal-free counter electrodes in high-performance DSSCs"
Angew. Chem. Int. Ed. 51, 12124-12127, 2012.

31. E. Iyyamperumal, S. Wang, L. Dai. "Vertically aligned BCN nanotubes with high capacitance"
    ACS Nano 6, 5259-5265, 2012.
32. Y. Xue, Y. Liu, F. Lu, J. Qu, H. Chen, L. Dai. "Functionalization of graphene oxide with polyhedral oligomeric silsesquioxane (POSS) for multifunctional applications"
    J. Phys. Chem. Lett. 3, 1607-1612, 2012.
33. N. Kumar, H.-J. Choi, Y.-R. Shin, D. W. Chang, L. Dai, J.-B. Baek. "Polyaniline grafted reduced graphene oxide for efficient electrochemical supercapacitors"
    ACS Nano 6, 1715-1723, 2012.
34. D. W. Chang, H.-J. Choi, S.-M. Jung, L. Dai, J.-B. Baek. "Large cluster and hollow microfibers by multicomponent self-assembling of citrate stabilized gold nanoparticles with temperature-responsive amphiphilic dendrimers"
    J. Mater. Chem. 22, 13365-13373, 2012.
35. D. Yu, Y. Xue, L. Dai. "Vertically-aligned carbon nanotube arrays co-doped with phosphorus and nitrogen as efficient metal-free electrocatalysts for oxygen reduction"
    J. Phys. Chem. Lett. 3, 2863-2870, 2012.
36. W. Lu, A. Goering, L. Qu, L. Dai. "Lithium-ion batteries based on vertically-aligned carbon nanotube electrodes and ionic liquid electrolytes"
    PhysChemChemPhys 14, 12099-12104, 2012.
37. J. Liu, Y. Xue, Y. Gao, D. Yu, M. Durstock, L. Dai. "Hole and electron extraction layers based on graphene oxide derivatives for high-performance bulk heterojunction solar cells"
    Adv. Mater. 24, 2227, 2012.
38. J. Liu, Y. Xue, L. Dai. "Sulfated graphene oxide as a hole-extraction layer in high-performance polymer solar cells"
    J. Phys. Chem Lett. 3, 1928-1933, 2012.

BOOK CHAPTERS

1. L. Qu, Y. Li and L. Dai *Gecko-Foot Mimetic Adhesion*, Chapter 9 in *Bioinspired Surface: Bioinspired Adhesion*, Ed. G. Swiegers, Ed., John Wiley & Sons, 2012.

2. M. Zhang, P. He and L. Dai *Biomedical Applications of Nanostructures: Carbon Nanotube Biosensors* in Carbon Nanomaterials Handbook, V. Presser and Y. Gogotsi, Eds., CRC Press, 2012.

3. J. Zhang, S. Zhang, Q. Dai, L. Dai *Heteroatom-Doped Carbon Nanotubes as Advanced Electrocatalysts for Oxygen Reduction Reaction* in Nanocarbons for Advanced Energy Conversion, Xinliang Feng, Ed., Wiley-VCH Verlag GmbH & Co., 2015.

III. PERSONNEL SUPPORT

PROJECT PARTICIPANTS

Senior Personnel
Liming Dai (PI, CWRU)

Post-doctors
Yonghua Chen (Full time, CWRU)
Jiantie Xue (Part time, CWRY)

AFRL Collaborators
Michael Durstock (WPAFB)

Throughout the project, close collaboration was maintained with Dr. Michael Durstock at AFRL/MLBP in Dayton. Dr. Dai and his team will continue to work closely together with Dr. Durstock's team to build a strong and long-term collaboration on energy initiatives to meet the Air Force needs.

IV. SIGNIFICANCE TO AIR FORCE AND CIVILIAN TECHNOLOGY CHALLENGES

Recent developments in military applications have placed renewed demands for advanced multifunctional nanomaterials and nanodevices, including new and improved high performance multifunctional dry adhesives, chemical/biological sensors, power generation and storage devices, and electrical/thermal management systems with significant improvements in weight to volume ratios. A strong fundamental understanding in the design, synthesis, and assembly of new hierarchically-structured nanotubes is critical in underpinning the development of novel technologies as well as providing opportunities for exploiting new scientific principles. This research project has brought together expertise and resources available at CWRU and AFRL. Throughout the program, close collaboration has been maintained with WPAFB in Dayton: particularly Michael Durstock's group at AFRX/WPAFB on the energy-related and other devices, including the chemical-/bio-sensors, dry/wet adhesives, and thermal and electrical managements. Over the past ten years or so, the PI has been collaborating with many AFRL researchers. His team has been working closely with AFRL on the proposed project to build a strong, long-term, and comprehensive network with AFRL. The interests of this proposal to Air Force are clearly evidenced by not only our many publications, including two *Science* papers, jointly published with researchers at WPAFB, but also a substantial amount of the proposed work that have been carried out in close collaboration with WPAFB researchers. The outcome of the proposed research directly supported the missions of AFOSR and AFRL, and the proposed work contributed significantly towards strengthening the national and Air Force capability for research and development of synthesis and fabrication of multifunctional materials and devices from VA-CNTs by: 1) providing Air Force with a scientific rationale that has led to innovations in the design of various lightweight and highly efficient smart devices for Air Force applications, 2) provided a body of information that allowed Air Force to design multifunctional VA-CNT systems to accomplish missions that are impossible with current materials/devices/methods, 3) trained post-doctoral students who can be expected to assume major responsibilities in critical defense-related research and development activities, and 4) brought together multidisciplinary expertise and resources in the area of nanomaterials synthesis and functionalization, characterization, and device design and construction from both CWRU and AFRL. The successful execution of this proposed project have impacted many Air Force assets and subcomponents, including pulsed-power, autonomous portable power,

small UAV propulsion and power, satellite power systems, chemical/biological sensors, wall/rock climbing robots, planet exploration, future military aircraft and space vehicles, and many other space systems where all conventional adhesives fail due to the vacuum environment in the space.

The outcomes of this project have also provided an opportunity for the domestic energy industry to create new jobs and strengthens the U.S. economy. This further enhanced our position to capture the economic and military benefits emerging from developments in this field. Our work has received numerous commentaries appeared in scientific, business, and popular press (please see: "Events & News" at http://case.edu/cse/eche/daigroup/news.html and many others on internet). Our technologies are envisioned to be transformative and having a large impact on the energy field, and their repercussions are continuing.

V. INTERACTIONS/TRANSITIONS

During this project period, the PI has been elected to be Fellows to the Royal Society of Chemistry and the American Institute of Medical and Biological Engineering and invited to serve as members of the Advisory Editorial Board for several international journals, including the *ACS Nano*, *Materials Research Express*, *ChemNanoMat*, and *Graphene Chemistry*, while the PI and team members have presented the results from this project at many national and international conferences, including:

2015 Plenary talk at the International Workshop on Graphene and C_3N_4-based Photocatalysts (IWGCP) to be held in Wuhan, China, June 5-8, 2015
Invited talk in the 250th ACS meeting (ENFL Division), Boston, Aug. 16-20, 2015,
Keynote talk at the Second International Conference on Electrochemical Energy Science and Technology (EEST2015), Vancouver, August 16th to 22nd, 2015
Invited talk at the NSTI Nanotech Conference, DC, June 14-17, 2015
Plenary talk at the 2nd China-USA symposium, Shanghai, June 27-28, 2015
Keynote talk at The 14th Pacific Polymer Conference, Kauai, Hawaii, Dec. 9-13, 2015

Co-Organizers for Symposium Energy: Graphene and Carbon Nanocomposites at The 14th Pacific Polymer Conference, Kauai, Hawaii on Dec. 9-13, 2015
Co-Organizers for the Advanced Materials and Nanotechnology Symposium at the Sino-US Chemical Engineering Conference, Shanghai, October 13-16, 2015
Co-Organizers for Symposium: "Nano Carbon Materials: From 1D to 3D" for the Fall 2015 MRS, Boston, November 29 to December 4, 2015

2014 Plenary lecture at the First International Conference on Polymer Science and Engineering (PSE-2014), Beijing, China, November 10-13, 2014
Invited talk at the Nanoenergy Nanosystems 2014 (NENS 2014), Beijing, China, Dec. 8-10, 2014
Invited talk at the 2014 MRS Spring Meeting, San Francisco, April 21-25, 2014
Invited talk at the 248th ACS National Meeting, San Francisco, August 10-14, 2014
Invited talk at the 247th ACS National Meeting, Dallas, March 16-20, 2014
Invited talk at the 225th meeting of The Electrochemical Society Orlando, May 12-15
Invited talk at Asia Pacific Conference on Electrochemical Energy Storage and Conversion, Brisbane, February 5-8, 2014

2013 Invited talk at the 7th Sino-US Conference of Chemical Engineering, Beijing,

October 14-18, 2013

Invited talk at the 246th ACS National Meeting, Indianapolis, Sept. 8-12, 2013

Invited keynote lecture at the 4th International Conference of Bionic Engineering (ICBE'13), Nanjing, August 13-16, 2013

Invited talk at the 245th ACS National Meeting, New Orleans, April 7-11, 2013

Invited talk at the 2013 International Photonics and OptoElectronics Meetings (POEM 2013), Wuhan, May 25-26, 2013

Invited talk at the 11th NANO KOREA, Seoul, July 10-12, 2013

Invited talk at the MACROFRONTIERS 2013, Cleveland, June 6-8, 2013

2012 Plenary talk at the OZ Carbon 2012 conference, Adelaide, July 1-3, 2012.

Invited talk at the Gordon Conference on the Chemistry and Physics of Graphitic Carbon Materials, Davidson College, NC, June 17-22, 2012.

Keynote talk at the 9th Annual Conference on FOUNDATIONS OF NANOSCIENCE: SELF-ASSEMBLED ARCHITECTURES AND DEVICES (FNANO12), Snowbird, Utah, April 16 –19, 2012.

Invited talk at the 244th ACS National Meeting, Philadelphia, Pennsylvania, August 19-23, 2012.

Invited talk at the IUPAC World Polymer Congress, Blacksburg, Virginia, June 24-29, 2012.

Invited talk at the 2012 US-Korea Joint Symposium of Nanotechnology, Dallas, Texas, May 1-4, 2012.

1.

1. Report Type

Final Report

Primary Contact E-mail

Contact email if there is a problem with the report.

liming.dai@case.edu

Primary Contact Phone Number

Contact phone number if there is a problem with the report

2163684176

Organization / Institution name

Case Western Reserve University

Grant/Contract Title

The full title of the funded effort.

Controlled Synthesis and Functionalization of Vertically-Aligned Carbon Nanotubes for Multifunctional Applications

Grant/Contract Number

AFOSR assigned control number. It must begin with "FA9550" or "F49620" or "FA2386".

FA9550-12-1-0069

Principal Investigator Name

The full name of the principal investigator on the grant or contract.

Liming Dai

Program Manager

The AFOSR Program Manager currently assigned to the award

Charles Lee

Reporting Period Start Date

05/01/2012

Reporting Period End Date

04/30/2015

Abstract

As we proposed originally, the objective of the project is to synthesize and functionalize vertically-aligned carbon nanotubes (VA-CNTs) for multifunctional applications. Along with the development of advanced CVD and solutions method for controlled synthesis of VA-CNTs, we have also develop leading-edge functionalization strategies to prepare VA-CNT with various tailor-made architectures/structures for a large variety of applications, including energy- (e.g., supercapacitors, batteries, solar cells, fuel cells) and bio-related devices (e.g., biosensors, biomimetic dry adhesives). This project has led to more than 38 journal publications, including Nature Nanotechnology (2), Angew. Chem. Int. Ed. (2), Advanced Materials (3), Energy Environ. Sci. (1), ACS Nano (3), Nano Lett. (1), Acc. Chem. Res. (1), and Chem. Rev. (1), 3 book chapters, and received numerous commentaries appeared in scientific, business, and popular press (please see: “Events & News” at http://case.edu/cse/eche/daigroup/news.html and many others on internet).

Distribution Statement

This is block 12 on the SF298 form.

Distribution A - Approved for Public Release

Explanation for Distribution Statement

If this is not approved for public release, please provide a short explanation. E.g., contains proprietary information.

SF298 Form

Please attach your SF298 form. A blank SF298 can be found here. Please do not password protect or secure the PDF The maximum file size for an SF298 is 50MB.

SF298 is attached to the final report (AF9550-12-1-0069).pdf

Upload the Report Document. File must be a PDF. Please do not password protect or secure the PDF . The maximum file size for the Report Document is 50MB.

Final Report (AF9550-12-1-0069)-LDai.pdf

Upload a Report Document, if any. The maximum file size for the Report Document is 50MB.

Archival Publications (published) during reporting period:

JOURNAL PAPERS PUBLISHED FROM THIS PROJECT WITH ACKNOWLEDGEMENTS TO THE AFOSR GRANT AND BOOK CHAPTERS

JOURNAL PUBLICATIONS

1. J. Zhang, Z. Zhao, Z. Xia, L. Dai. "A metal-free bifunctional electrocatalyst for oxygen reduction and oxygen evolution reactions"
Nat Nanotechnol. DOI:10.1038/nnano.2015.48, 2015.
2. L. Dai, Y. Xua, L. Qu, H.-J. Choi, J.-B. Baek. “Metal-Free Catalysts for Oxygen Reduction Reaction”
Chem. Rev. 2015, DOI: 10.1021/cr5003563.
3. T. Chen, R. Hao, H. Peng, L. Dai. “High-performance, extremely stretchable, wire-shaped supercapacitors”
Angew. Chem. Int. Ed. 54, 618–622, 2015.
4. J. Xu, M. Wang, N. P. Wickramaratne, M. Jaroniec, S. Dou, L. Dai. "High-Performance Sodium Ion Batteries Based on Three-Dimensional Anode from Nitrogen-Doped Graphene Foams"
Adv. Mater .27, 2042-2048, 2015.
5. Z. Xiang, D. Cao, L. Dai. "Well-Defined Two Dimensional Covalent Organic Polymers: Rational Design, Controlled Syntheses, and Potential Applications"
Polym. Chem. 6, 1896-1911, 2015.
6. I.-Y. Jeon, M.J. Ju, J. Xu, H.-J. Choi, J.-M. Seo, M.-J. Kim, I. T. Choi, H.M. Kim, J.C. Kim, J.-J. Lee, H. K. Liu, H.K. Kim, S. Dou, L. Dai, J.-B. Baek. “Edge-Fluorinated Graphene Nanoplatelets as High Performance Electrodes for Dye-Sensitized Solar Cells and Lithium Ion Batteries”
Adv. Funct. Mater. 25, 1170-1179, 2015.
7. Y. Xue, J.M. Baek, H. Chen, J. Qu, L. Dai. "N-doped graphene nanoribbons as efficient metal-free counter electrode for disulfide/thiolate redox mediated DSSCs"
Nanoscale 7, 7078-7083, 2015.
8. Y. Xue, L. Zhu, H. Chen, J. Qu, L. Dai. “Multiscale patterning of graphene oxide and reduced graphene oxide for flexible supercapacitors” Carbon (2015) DOI: org/10.1016/j.carbon.2015.04.046.
9. J. Liu, M. Durstock, L. Dai. "Graphene oxide derivatives as hole- and electron-extraction layers for high-performance polymer solar cells"
Energy Environ. Sci. 7, 1297-1306, 2014.
10. D. Yu, K. Goh, H. Wang, L. Wei, W. Jiang, Q. Zhang, L. Dai, Y.Chen. "Scalable synthesis of hierarchically-structured carbon nanotube-graphene fibres for capacitive

energy storage"
Nat. Nanotechnol. 9, 555–562, 2014.
11. T. Chen, H. Peng, M. Durstock, L. Dai. "High-performance transparent and stretchable all-solid supercapacitors based on highly aligned carbon nanotube sheets"
Sci. Rep., 4, 3612, 2014.
12. Y. Chen, W.-C. Lin, J. Liu, L. Dai. "Graphene oxide-based carbon interconnecting layer for high-performance polymer tandem solar cells"
Nano Lett., 14 (3), 1467–1471, 2014.
13. J. Xu, I.-Y. Jeon, J.M. Seo, S. Dou, L. Dai, J.-B Baek. "Edge-selectively halogenated graphene nanoplatelets (XGnPs, X = Cl, Br, or I) prepared by ball-milling and used as anode materials for lithium-ion batteries"
Adv. Mater. 26, 7317–7323, 2014.
14. N. P. Wickramaratne, J. Xu, M. Wang, L. Zhu, L. Dai, M. Jaroniec. "Nitrogen enriched porous carbon spheres: Attractive materials for supercapacitor electrodes and CO2 adsorption"
Chem. Mater. 26, 2820–2828, 2014.
15. J. Xu, J. Shui, J. Wang, M. Wang, H.-K. Liu, S.X. Dou, I.-Y. Jeon, J.-M. Seo, J.-B. Baek, L. Dai. "Sulfur-graphene nanostructured cathodes via ball-milling for high-performance lithium-sulfur batteries"
ACS Nano 8, 10920-10930, 2014.
16. D. Wang, J. Chen, L. Dai. "Recent advances in graphene quantum dots for fluorescence bioimaging from cells through tissues to animals"
Particle & Particle Systems Characterization, DOI:10.1002/ppsc.201400219, 2014.
17. J. Liu, M. Durstock, L. Dai. "Graphene oxide derivatives as hole- and electron-extraction layers for high-performance polymer solar cells"
Energy & Environmental Science 7, 1297-1306, 2014.
18. J. Shui, F. Du, C. Xue, Q. Li, L. Dai, "Vertically aligned N-doped coral-like carbon fiber arrays as efficient air electrodes for high-performance non-aqueous Li-O2 batteries"
ACS Nano 8 (3), 3015–3022, 2014.
19. T. Chen, L. Dai, "Flexible supercapacitors based on carbon nanomaterials"
J. Mater. Chem. A, 2, 10756-10775, 2014.
20. L. Xiang, P. Yu, Y. Wang, M. Zhang, L. Zhu, L. Dai, L. Mao. "Platinized aligned carbon nanotube-sheathed carbon fiber microelectrodes for in vivo amperometric monitoring of oxygen"
Anal. Chem. 86, 5017-5023, 2014.
21. L. Dai. "Functionalization of graphene for efficient energy conversion and storage"
Acc. Chem. Res. 46, 31-42, 2013.
22. W. Lu, L. Dai. "Carbon nanotubes for advanced energy conversion and storage"
J. Nano Energy Power Res. 2, 1-24, 2013.
23. I.-Y. Jeon, H.-J. Choi, M. J. Ju, I. T. Choi, K. Lim, J. Ko, H. K. Kim, J. C. Kim, J. J. Lee, D. Shin, S.-M. Jung, J.-M. Seo, M.-J. Kim, N. Park,L. Dai, J.-B. Baek. "Direct nitrogen fixation at the edges of graphene nanoplatelets as efficient metal-free electrocatalysts for energy conversion"
Scientific Reports 3, 2260, 2013.
24. T. Chen, L. Dai. "Carbon nanomaterials for high-performance supercapacitors"
Materials Today 16, 272-280, 2013.
25. J. Liu, Y. Xue, M. Zhang, L. Dai. "Graphene-based materials for energy applications"
MRS Bull. 37, 1265-1272, 2013.
26. I.-Y. Jeon, H.-J. Choi, M. Choi, J.-M. Seo, S.-M. Jung, M.-J. Kim, S. Zhang, L. Zhang, Z. Xia, L. Dai, N. Park, J.-B. Baek. "Facile, scalable synthesis of edge-halogenated graphene nanoplatelets as efficient metal-free eletrocatalysts for oxygen reduction reaction"
Scientific Reports 3, 1810, 2013.

27. Y. Xue, D. Yu, L. Dai, R. Wang, D. Li, A. Roy, F. Lu, H. Chen, Y. Liu, J. Qu."Three-dimensional B, N-doped graphene foam as metal-free catalysts for oxygen reduction reaction"
Phys.Chem.Chem. Phys. 15, 12220-12226, 2013.
28. J. Xu, S. Dou, H. Liu, L. Dai. "Cathode materials for next generation lithium ion batteries"
Nano Energy 439-442, 2013.
29. I.-Y. Jeon, Y.-R. Shin, G.-J. Sohn, H.-J. Choi, S.-Y. Bae, J. Mahmood, S.-M. Jung, J.-M. Seo, M.-J. Kima, D. W. Chang, L. Dai, and J.-B. Baek. "Edge-carboxylated graphene nanosheets via ball milling"
Proc. Natl. Acad. Sci. USA 109, 5588-5593, 2012.
30. Y. Xue, J. Liu, H. Chen, R. Wang, D. Li, J. Qu, L. Dai. "Nitrogen-doped graphene foams as metal-free counter electrodes in high-performance DSSCs"
Angew. Chem. Int. Ed. 51, 12124-12127, 2012.
31. E. Iyyamperumal, S. Wang, L. Dai. "Vertically aligned BCN nanotubes with high capacitance"
ACS Nano 6, 5259-5265, 2012.
32. Y. Xue, Y. Liu, F. Lu, J. Qu, H. Chen, L. Dai. "Functionalization of graphene oxide with polyhedral oligomeric silsesquioxane (POSS) for multifunctional applications"
J. Phys. Chem. Lett. 3, 1607-1612, 2012.
33. N. Kumar, H.-J. Choi, Y.-R. Shin, D. W. Chang, L. Dai, J.-B. Baek. "Polyaniline grafted reduced graphene oxide for efficient electrochemical supercapacitors"
ACS Nano 6, 1715-1723, 2012.
34. D. W. Chang, H.-J. Choi, S.-M. Jung, L. Dai, J.-B. Baek. "Large cluster and hollow microfibers by multicomponent self-assembling of citrate stabilized gold nanoparticles with temperature-responsive amphiphilic dendrimers"
J. Mater. Chem. 22, 13365-13373, 2012.
35. D. Yu, Y. Xue, L. Dai. "Vertically-aligned carbon nanotube arrays co-doped with phosphorus and nitrogen as efficient metal-free electrocatalysts for oxygen reduction"
J. Phys. Chem. Lett. 3, 2863-2870, 2012.
36. W. Lu, A. Goering, L. Qu, L. Dai. "Lithium-ion batteries based on vertically-aligned carbon nanotube electrodes and ionic liquid electrolytes"
PhysChemChemPhys 14, 12099-12104, 2012.
37. J. Liu, Y. Xue, Y. Gao, D. Yu, M. Durstock, L. Dai. "Hole and electron extraction layers based on graphene oxide derivatives for high-performance bulk heterojunction solar cells"
Adv. Mater. 24, 2227, 2012.
38. J. Liu, Y. Xue, L. Dai. "Sulfated graphene oxide as a hole-extraction layer in high-performance polymer solar cells"
J. Phys. Chem Lett. 3, 1928-1933, 2012.

BOOK CHAPTERS

1. L. Qu, Y. Li and L. Dai Gecko-Foot Mimetic Adhesion, Chapter 9 in Bioinspired Surface: Bioinspired Adhesion, Ed. G. Swiegers, Ed., John Wiley & Sons, 2012.

2. M. Zhang, P. He and L. Dai Biomedical Applications of Nanostructures: Carbon Nanotube Biosensors in Carbon Nanomaterials Handbook, V. Presser and Y. Gogotsi, Eds., CRC Press, 2012.

3. J. Zhang, S. Zhang, Q. Dai, L. Dai Heteroatom-Doped Carbon Nanotubes as Advanced

Electrocatalysts for Oxygen Reduction Reaction in Nanocarbons for Advanced Energy Conversion, Xinliang Feng, Ed., Wiley-VCH Verlag GmbH & Co., 2015.

Changes in research objectives (if any):

NIL

Change in AFOSR Program Manager, if any:

NIL

Extensions granted or milestones slipped, if any:

NIL

AFOSR LRIR Number

LRIR Title

Reporting Period

Laboratory Task Manager

Program Officer

Research Objectives

Technical Summary

Funding Summary by Cost Category (by FY, $K)

	Starting FY	FY+1	FY+2
Salary			
Equipment/Facilities			
Supplies			
Total			

Report Document

Report Document - Text Analysis

Report Document - Text Analysis

Appendix Documents

2. Thank You

E-mail user

Apr 28, 2015 11:43:43 Success: Email Sent to: liming.dai@case.edu